CATALYTIC METHANOL COMBUSTION

A Thesis Submitted to
The Graduate School of Engineering and Sciences of
Izmir Institute of Technology
In Partial Fulfillment of the Requirements for the Degree of

MASTER OF SCIENCE

in Chemical Engineering

by
Emre DEMİRKAYA

July 2015
İZMİR

We approve the thesis of **Emre DEMİRKAYA**

Examining Committee Members:

_____

Doç. Dr. Erol ŞEKER
Department of Chemical Engineering, Izmir Institute of Technology

_____

Prof. Dr. Sacide ALSOY ALTINKAYA
Department of Chemical Engineering, Izmir Institute of Technology

_____

Prof. Dr. Oğuz BAYRAKTAR
Department of Chemical Engineering, Ege University

28 July 2015

_____

Doç. Dr. Erol ŞEKER
Supervisor, Department of Chemical Engineering,
Izmir Institute of Technology

_____

Prof. Dr. S. Fehime ÇAKICIOĞLU ÖZKAN
Head of the Department of Chemical Engineering

_____

Prof. Dr. Bilge KARAÇALI
Dean of the Graduate School of Engineering and Sciences

ACKNOWLEDGEMENTS

I am really thankful to people who made this thesis possible.

I would like to express my gratefulness to my MSc supervisor Assoc. Prof. Erol ŞEKER for his encouragement, guidance, sound advices, patience and lots of good ideas that he shared with me.

I also appreciate to Prof. Dr. Mehmet POLAT that he leads the way to us having a chance in doing Master's degree in Chemical Engineering Department, encouragement and good advices.

It's a pleasure for me to thank Merve ÖZPİRİN for helping me get through the difficult times, limitless support, her friendship, emotional support and caring throughout this study.

I wish to thank to all my friends and colleagues; Gizem PAYER, H. Arda YURTSEVER, Selcan ATEŞ, Sema KIRKÖSE, Dildare METİN BAŞALP, Vahide NURAN ÖZGÜR, Emre KILIÇ, Mert TUNÇER and Esra TUZCUOĞLU for their help and friendship.

Finally, my special thanks goes to my family, for their endless support throughout my life and helping me always to get through the difficult times.

ABSTRACT

CATALYTIC METHANOL COMBUSTION

Throughout this study, the major goal is to analyze the product distribution of methanol combustion at different reaction conditions, such as, varying space velocities, different initial temperatures, on 2% Pt/Al_2O_3 catalyst. The catalyst support material, alumina, was prepared by using a single-step sol-gel method and platinum was added by using the impregnation method. The reaction was conducted in a tubular reactor.

In this work, the maximum steady state temperature at room temperature experiment was achieved almost same within the error for 2.4 s^{-1} and 2.8 s^{-1} space velocity for fresh catalyst, and also, the conversion to CO_2 during the methanol combustion reaction for all the space velocities (2.4 s^{-1}, 2.8 s^{-1} and 3.1 s^{-1}) were found to be ~100%. Another parameter that was studied was the temperatures below the room temperature. The reaction was performed at -13^oC, 0^oC, 7^oC and 15^oC temperatures. With decreasing initial temperature, the steady state temperature was also found to be decrease. This was correlated with the product distribution and with decreasing initial temperature, CO_2 conversion decrement was observed..

Methyl formate was detected to be the main byproduct that was produced under all the space velocities at temperatures lower than room temperatures. The catalyst was active even at -13^oC. Therefore, it showed that it could be used as a catalyst for an external heater to provide necessary heat to reach the direct methanol fuel cells operating temperature at and below room temperature. Other than the other catalysts that was investigated in literature, our catalyst does not need to heat up the reactor. Once the fuel is supplied, the system reaches the necessary operating temperature by itself. This is desirable especially in portable DMFCs. The catalytic methanol combustion system investigated in this study seems to be promising to easily replace the lithium-ion batteries for portable electronic systems, especially ones used in the military.

ÖZET

KATALİTİK METANOL YANMASI

Bu çalışma süresince metanolün, değişik alan hızı ve ortam sıcaklığı gibi değişik koşullarda %2'lik alumina destekli platin katalizör üzerinde yanması incelenmiştir. Çalışmanın amacı değişik koşullardaki ürün dağılımını gözlemlemektir. Katalizör destek malzemesi, alumina, tek basamaklı sol-jel metodu ile hazırlanmıştır ve üzerine platin takviyesi doyurma yöntemiyle gerçekleştirilmiştir. Reaksiyon tübüler reaktörde gerçekleştirilmiştir.

Bu çalışmada, oda sıcaklığında yapılan deneylerde, maksimum denge durumu sıcaklığına, ilk defa kullanılan katalizör için, saniyede 2.4 ve 2.8 alan hızında ulaşılmıştır, fakat üç değişik alan hızı için de ($2.4\ s^{-1}$, $2.8\ s^{-1}$ ve $3.1\ s^{-1}$) karbondioksite olan dönüşümün yüzde 100 olduğu bulunmuştur.

Çalışılan diğer parametreler ise oda sıcaklığının altındaki sıcaklıklardır. Bu anlamda, tepkimeler -13^oC, 0^oC, 7^oC ve 15^oC sıcaklıklarda gerçekleştirilmiştir. Azalan giriş sıcaklıklarıyla (ortam sıcaklıkları) birlikte, denge durumuna ulaşan maksimum sıcaklıkların da azaldığı gözlemlenmiştir. Bu durum ürün dağılım analiziyle beraber kanıtlanmaya çalışılmıştır ve azalan ortam sıcaklığıyla beraber, karbondioksite dönüşme oranının da azaldığı gözlemlenmiştir.

Metil format tüm reaksiyonlarda ara ürün olarak tespit edilmiştir. -13^oC'de bile katalizörün gösterdiği aktivite doğrudan metanol yakıt hücrelerinin çalışma sıcaklığını sağlayabilecek bir dış ısıtıcı kaynağı olarak kullanılabileceğini göstermiştir. Literatürde çalışılan diğer katalizörlerden farklı olarak, bu çalışmada yer alan katalizörün reaktörünün ısıtılmasına ihtiyaç duyulmamıştır. Yakıt sağlandığı sürece sistem kendiliğinden direk metanol yakıt hücresinin çalışma sıcaklığına ulaşmaktadır. Bu özellike taşınabilir direk metanol yakıt hücreleri için arzulanan bir sonuçtur. Çalışılan sistem, taşınabilir elektronik sistemler için, özellikle askeri alanda, lityum iyon pillerinin yerini rahatlıkla alabilecek özelliktedir.

TABLE OF CONTENTS

LIST OF FIGURES

Figure **Page**

LIST OF TABLES

Table **Page**

CHAPTER 1

INTRODUCTION

World primary energy demand continues to increase between 2015 and 2035. Intervention of the governments affects the energy market and can change the energy trends in the long term. But, because of the some fundamental trends, like rising incomes and increment of the population, fossil fuel domination of global energy needs and dynamics of the energy markets effect directs the energy demands. According to World Energy Outlook (WEO), expectation of global economy expansion about 140% and rising of the world's population close to 9 billion until 2035 are two main factors that drive increment of the energy demand (WEO, 2012). Also, fast growing urbanization and industrial production mostly in non-Organization for Economic Cooperation and Development (non-OECD) countries result with the higher energy needs. Since it has been a tradition to handle the oil, coal and recently natural gas, which are easier to process with respect to the renewable energy types, their fuel mix are expected to meet the most of the world's energy needs in 2035, too (WEO, 2012).

Oil demand with the implementation of the new policies and subsidies, is anticipated to rise regularly from 84 to 97 million barrels per day until 2035, but is expected to fall its share in total world primary energy demand from about 32% to 27% between 2011 and 2035 (WEO, 2012). To balance much of the oil demand growth, particularly in non-OECD countries which have the higher increment on oil share, some measures like tax raise on oil products, switching to renewable fuels, reduction on subsidies, promotion of more efficient oil use and different policies especially in the transportation sector is taking into account. In transportation sector, passenger light-duty vehicles (PLDVs) are the biggest part of the transport demand which causes the much of the growth of the global oil demand. However, the government policies and measures for PLDVs are much more than the measures for the trucks today. Considering the fast increment of the road freight demand, oil demand can be curbed more efficiently with practicing some measures for trucks, either (WEO, 2012). In addition to the measures that mentioned above, fast extinction of oil sources and higher

prices of oil is responsible for slowdown of the oil demand growth and the decrement of oil's share (BP Energy Outlook 2030, 2013).

Another fossil fuel, coal, is expected to come after oil as a second primary fuel despite a few percentage loss where natural gas share boosts until 2035 (WEO, 2012). Especially in non-OECD countries coal usage is indispensable in power sector. Gigantic coal demand growth in China between 1999 and 2011 was lead to the share of coal in the global primary energy mix increment up to 28%. In rising economies, in particular China and India, coal-fired power generation is responsible for this huge coal demand growth. With the well-designed policy actions this trend can be reversed. China's coal demand around 2020 has its maximum and goes stable through 2035 and leads half of global increasing coal demand over this period (WEO, 2012). India, by 2025, becomes the second larger coal consumer with overtaking United States. In contrast, in OECD countries coal demand shows a decrement, especially in Europe. By 2020 through 2035, China's coal demand stabilization, slowing down the growth in other non-OECD countries and decreasing of the coal demand in OECD countries result with the share of coal in world primary energy demand stay around 25% (WEO, 2012).

Despite decreasing share of coal and oil between 2011 and 2035, natural gas shows increment and gains share steadily. It is expected that, natural gas consumption approach from 3.4 trillion cubic meters (tcm) in 2011 to around 5 tcm in 2035. Since natural gas is the least carbon-intensive fossil fuel, its utilization is not much affected by policies to decelerate global warming in contrast to the coal and oil. Also, extensive gas sources existence keeps gas prices competitive. These two important factors explain higher demand and share growth of the natural gas (WEO, 2012).

Due to the drawbacks of the fossil fuels that talked above and increasing understanding of the importance of renewable energy, made significant improvement on research and development on this type of energy. Also, implementation of environmental policies and subsidies by governments helps more to increase the share of the use of renewable energy sources, like, hydro, solar, wind, bioenergy and geothermal. In addition to that, until 2035, electricity generation from renewables is expected to be triple times more than in 2011, means that about 31% of total generation all over the world (WEO, 2012). Among the all renewable energy sources, hydro is the major renewable source for power generation globally, now. Even if its electricity generation increases from 3,431 terawatts-hour (TWh) to 5,677 TWh, between 2010 and 2035, its share in total produced electricity is not expected to be changed much as

around 16%. Conversely, wind power becomes more cost competitive with the government policy supports to produce electricity. It continues to spread out quickly and its share in total produced electricity can be around 7.3%, in 2035, globally. However, there are still significant uncertainties about the offshore wind costs, in comparison with the onshore wind costs. Offshore wind costs stays well over gross electricity prices in lots of countries. Onshore wind is responsible for the growth about four-fifths of total. Solar photovoltaics (PV) capacity is increasing very fast. Global solar PV capacity was increased from 1 gigawatts (GW) to 67 GW between 2000 and 2011. Only in 2011, it was showed an increment about 30 GW, about 75% increase. This huge increment was because of the significant falling down of the solar PV generating costs. A 44% decrement was experienced between the first quarters of 2010 and 2012. Also, installation of solar PV growth especially in European Union countries must be thankful to the feed-in tariffs that substantially decrease the risk of the projects and guarantees the returns. So, we can say that owing to these tariffs, the installation and generation costs of solar PV are not reflects the real costs. Therefore, a decrement of solar PV capacity growth and possible increases in electricity prices can be expected. Giving an importance to research and development of solar PV technology will lead to the reflection of the real costs (WEO, 2012).

Even though there is a significant increment on the technology and research and development of the renewable energy, there are some drawbacks in each type of renewable energy by itself. Also, although there is a considerable decrement on production cost of power from renewables, their cost is still higher than the non-renewable energy sources (WEO, 2012). In addition to that, renewable energy resources supplying nature is unsteady, yet. Considering these problems explains why renewables cannot fully replace the current fossil fuel sovereignty in the long run. On the other hand, hydrogen energy is a better option to replace fossil fuel economy domination since hydrogen can easily be produced from both renewable and non-renewable energy sources. In this manner, fuel cells are becoming to play an important role in the world where they are known as a better technology option than batteries or traditional internal combustion engines (Fuel Cell Today, 2013). Globally, research and development on fuel cells is expected to rise from 10% to 34% between 2008 and 2018. High emission levels, low energy efficiencies, fast extinction of resources and high cost of fossil fuels promote fuel cells commercialization. Therefore, especially in the industrialized countries rapid increment on sales is expecting over the coming decade (World Fuel

Cells, 2009). Adaptation of fuel cell technology substantially increases in China, United States, Western European countries, South Korea, Japan and Canada. Regionally, in last years, Asian countries have been the most important implementer of fuel cell technology. Only throughout 2012, Asian countries shipments exceeded the 75% of total fuel cell systems (Fuel Cell Today, 2012).

Fuel cell is basically a device that converts hydrogen and oxygen into electricity, water and heat electrochemically. It's an electrochemical energy conversion device, unlike batteries, as long as a fuel is supplied they can continuously generate electricity (Curtin et. al., 2013). In spite of having analogous components and some characteristics, fuel cells are different from a typical battery in many respects. Batteries are energy storage devices which determine the maximum available energy by the stored chemical reactant amount in itself. Meaning that, batteries consumes chemical reactants to produce electrical energy and then, (rechargeable batteries) from an external source gains the energy needed to regenerate the reactants by recharging. However, fuel cells have the ability of generating electrical energy if fuel and oxidant are supplied to the electrodes continuously (Behling, 2013). Working with the pure hydrogen fuel cells are basic and pollution free, they produce only electricity, water and heat (Web-1). On the other hand, if fossil fuels are used to produce hydrogen, fuel cell power plants can release CO_2 emissions. In fuel cell systems there is no combustion process that generates NO_x. All fuel cells can be poisoned by sulfur so it must be removed from the supplied fuel not to produce SO_x. No combustion process in fuel cell systems leads to no ash or large volume waste products. Fuel cells are not limited by Carnot efficiency so that gives them high efficiency characteristic. Efficiencies can be quite high as around between 55% - 65%. Even the strictest 2000 California standards were at least 10 times higher than the fuel cell power plant emissions. In addition to that, fuel cell power plants needs lower amounts of water in comparison with any steam power plants, since they produce water as a by-product. Also, this water is clean and a pretreatment process is not necessary to use it again. Having no moving parts in fuel cells and very few moving parts in the entire system makes them reliable. On the other hand, material degradation can occur because of the presence of reactants, various operating conditions such as high temperature and pressures, and catalytic materials. Since these are not costly, they don't cause problems in maintenance that much. When we compare fuel cell power plants and steam or gas power plants, fuel cell power plant will be found as

quieter, because noise is generated only from ancillary units like fans, compressors, pumps, etc. (Shah, 2007).

Fuel cell applications and technologies categorizes into three wide areas. Portable fuel cells exists of moving fuel cell systems, stationary fuel cells are designed to be at a fixed location to generate power and transport fuel cells provide either propulsive power or range-extension capability to vehicles. Table 1.1 shows some details about these applications and technologies. APU, laptops, mobile phones, night vision goggles, navigation devices and radios are examples of portable fuel cells applications. Uninterruptible power supply (UPS), residential power and combined heat and power (CHP) are applications of stationary fuel cells. Fuel cell electric vehicles and auxiliary power units can be found in transportation applications of fuel cells (Fuel Cell Today, 2012). In unit shipments, portable fuel cells dominated the market as having over 70% of global unit sales in 2013. But, in terms of installed capacity stationary fuel cells was found as dominating as compared to the portable fuel cells since portables have smaller size that leads to lower installed capacity of them (Grand View Research, 2014). Although the dominance of portables in terms of unit shipments was took place in 2013, there was a slight decrement with respect to the unit shipments in 2012. This is just because of the delay of two corporations fuel cell systems start as not planned and the third one, which reached to the consumer market, adoption was considerably lower than expected. Increment in unit shipments of portables is expected to continue in next years (Fuel Cell Today, 2012).

Table 1.1. Fuel Cell applications and technologies.
(Source: Fuel Cell Today, 2013)

	Portable	Stationary	Transport
Definition	Units that are designed to be moved, including auxiliary power units (APU)	Units that are provide electricity, sometimes heat, but not designed to be moved	Units that provide propulsive power or range extension to a vehicle
Power Range	5 to 20 kW	0.5 to 400 kW	1 to 100 kW
Typical technology	PEMFC - DMFC	MCFC – PEMFC PAFC – SOFC	PEMFC - DMFC
Examples	Non-motive APU (campervans, boats); military applications (portable soldier-borne power, skid-mounted generators); portable products (torches, battery chargers), small personal electronics (mp3 players, cameras)	Large stationary combined heat and power (CHP); small stationary micro-CHP; uninterruptible power supplies (UPS)	Materials handling vehicles; fuel cell electric vehicles (FCEV); Trucks and buses

Fuel cells can be classified with respect to the different criteria. This criteria would be fuel type, oxidizer type, electrolyte type, charge carrier or temperature. Even though, the most common classification is by their electrolyte type, they are usually classified by the fuel type, too. The major fuel cell technology types are; phosphoric acid fuel cells (PAFC), proton exchange membrane fuel cells (PEMFC), solid oxide fuel cells (SOFC), direct methanol fuel cells (DMFC), alkaline fuel cells (AFC) and molten carbonate fuel cells (MCFC) (Shah, 2007). Some characteristics of fuel cell types are as shown in Table 1.2.

Table 1.2. Types of fuel cells and their features.
(Source: Shah, 2007)

	PEMFC	DMFC	AFC	PAFC	MCFC	SOFC
Primary applications	Automotive and stationary power	Portable power	Space vehicles and drinking water	Stationary power	Stationary power	Vehicle auxiliary power
Electrolyte	Polymer (plastic) membrane	Polymer (plastic) membrane	Concentrated (30-50%) KOH in H_2O	Concentrated 100% phosphoric acid	Molten carbonate retained in a ceramic matrix of $LiAlO_2$	Yttrium-stabilized Zirkondioxide
Operating Temperature	~100°C	~60°C	~200°C	~220°C	~700°C	~1000°C
Charge carrier	H^+	H^+	OH^-	H^+	CO_3^{-2}	O^{-2}
Prime cell components	Carbon based	Carbon based	Carbon based	Carbon based	Stainless steel	Ceramic
Catalyst	Platinum	Pt-Pt/Ru	Platinum	Platinum	Nickel	Perovskites
Primary fuel	H_2	Methanol	H_2	H_2	H_2, CO	H_2, CO, CH_4
Start-up time	Sec-min	Sec-min		Hours	Hours	Hours
Power density (kW/m3)	3.8-6.5	~0.6	~1	0.8-1.9	1.5-2.6	0.1-1.5
Combined cycle fuel cell efficiency	50-60%	30-40% (no combined cycle)	50-60%	55%	55-65%	55-65%

A fuel cell includes anode, anodic catalyst layer, electrolyte, cathodic catalyst layer, cathode, bipolar plates or interconnects and occasionally gaskets for sealing to prevent leak of gases between anode and cathode. Each fuel cell can connect to each other in serial or in parallel or in both to generate the desired voltage and current. Different types of catalysts can be used depending on the fuel cell type. Platinum, is an example for low temperature fuel cells and nickel is for high temperature fuel cells, most commonly. The charge carriers changes with respect to the fuel cell types. To collect the electrical current, and also, to distribute and separate the reactive gases in the fuel cell stack, bipolar plates (interconnects) uses (Shah, 2007).

As long as fuel and oxidant are supplied to the electrodes, electrons or ions produce or consume and electrochemical reaction occurs. On the anode electrons are

produced and on the cathode electrons are consumed. An external circuit helps to move electrons from anode to cathode. Ions flow between anode and cathode within the fuel cell. Electrolyte enables the continuous ion creation and also behaves like a physical barrier to prevent the fuel and oxidant gas streams mixing. The simplest operation of a fuel cell is that fuel flows into the fuel cell and through the porous anode, fuel atoms separates into protons and electrons with the help of a catalyst and these electrons flow to the electrical circuit to generate electrical power. The protons flow through the electrolyte to the cathode and by the way oxidant sends into the fuel cell and then to the cathode. The cathode's catalyst combines protons, electrons and oxidant to produce the product. The schema of a fuel cell was shown as in Figure 1.1.

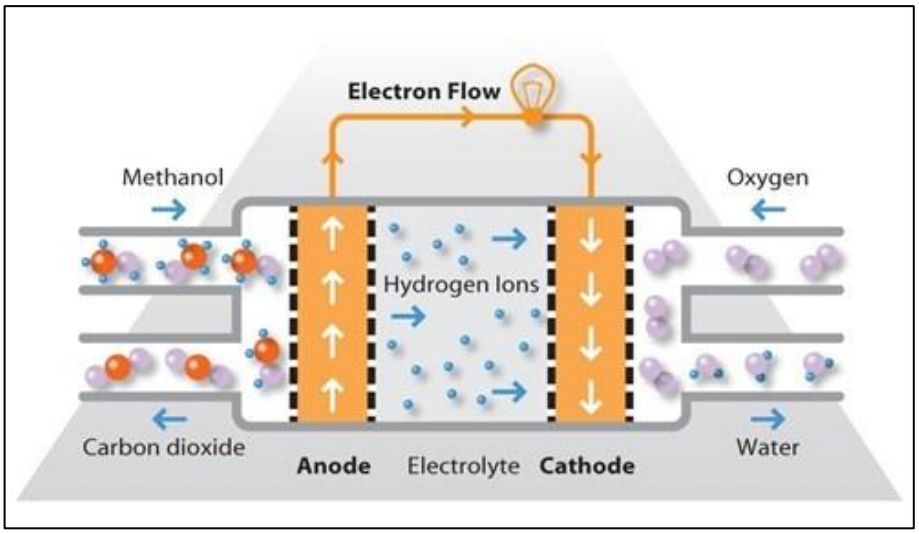

Figure 1.1. Schematic of a fuel cell.
(Source: Behling, 2013)

One of the most focused areas was the direct electrochemical oxidation of alcohol and hydrocarbon fuels. Organic liquid fuels are known as their high energy density, one of them, methanol is one step ahead with its remarkable characteristics as its reactivity even at low temperatures, storage and handling ease. Considering the rapid development of the DMFCs, methanol has a significant importance as a fuel. With respect to other fuel options, methanol is cheap and infrastructure for usage as a liquid fuel is sufficient. It can be provided from fossil fuels and also from sustainable resources. Unlike ethanol, methanol has high selectivity to carbon dioxide production in

the electrochemical oxidation processes (Arico et al., 2009; Srinivasan et al., 2006). Since methanol has an extensive high energy density (~20 MJ/kg) in comparison with the lithium-ion batteries (~0.9 MJ/kg), for portable applications DMFC can take place whole batteries in future (Spearrin, 2012). However, some drawbacks exist about DMFCs, like having low power density and low efficiency than PEMFCs. Since slow oxidative reaction kinetics of methanol and slow crossover it from anode to the cathode, electrical performance decreases below 60^{o}C (Liu and Zhang, 2009; Nakagawa, 2003) about 5 times, and there is an external heater requirement for the low temperature start-ups since it cannot be operated below 50^{o}C. Even though, DMFCs have high importance especially in portable type, such as power source for communication devices, radios, night vision goggles, laptops, navigation, etc. in military (Fuel Cell Today, 2013).

The objective of this thesis is to investigate the product distribution of the catalytic oxidation of methanol at low temperatures and three different space velocities in the manner of using as an external heater to reach at the temperature of ~60^{o}C , a typical DMFC operating temperature, over aluminum oxide supported platinum catalysts (Pt/Al_2O_3) that prepared using incipient wetness impregnation method and modified single step sol-gel made alumina.

This thesis consists of five chapters. In the first chapter, global energy consumption and demand with respect to the different fuel types are mentioned and some brief information about the future energy trends, new energy sources and the fuel cells features, operating principles and types, particularly DMFC, is given. Past studies about the catalytic methanol oxidation over metal oxide catalysts (supported/unsupported) and noble metal catalysts (supported/unsupported) are presented in details in literature survey in Chapter 2. Specification of the chemicals, catalyst preparation, characterization and activity tests that is performed experimentally are explained in Chapter 3. Chapter 4 is included results and discussion of the performance and the product distribution of the catalysts at different start-up temperatures for varying residence times. Lastly, conclusions and recommendations are given in Chapter 5.

CHAPTER 2

LITERATURE SURVEY

2.1. Methanol and Methanol Oxidation

For DMFC, methanol is the fuel, we can benefit the heat release from the oxidation of methanol as an external heat source. Methanol like other VOCs can be oxidized thermally and catalytically. Thermal oxidation requires higher temperatures, 1000^{o}C and higher, whereas the catalytic oxidation can operate at much lower temperatures. Therefore, the byproducts of the methanol combustion don't produce NO_x, SO_x and particulate matters (PMs). Also less energy is required for catalytic oxidation of methanol as compared to the thermal oxidation. These make the catalytic oxidation more environmentally friendly.

In literature, several studies were performed to research the activity of the catalysts and to improve them to find the most active catalyst / best catalyst formulation for VOC oxidation. In 1987, Spivey mentioned about the general conclusions made up to 1987 about the catalytic oxidation of VOCs. It was referred that, for the complete oxidation of VOCs, both metal oxides and noble metals are active. Also, in this type of oxidation, for metal oxides, surface oxygen and lattice takes place, and for supported noble metals, reduced metal sites play a role in the mechanism.

Also, Spivey referred that, the type of the catalyst determines the mechanism of complete catalytic oxidation. Since large excess amount of oxygen is the most preferred, oxygen concentration on the catalyst surface is mostly high. Therefore, that make us to assume the oxygen concentration in the gas phase is constant and led to the overall rate as the only function of VOC concentration (Spivey, 1987). Another point that dealt with in this study was the noble metal catalysts are most preferred catalysts for non-halogenated VOC oxidation while metal oxide catalysts are for halogenated VOCs. This result was approached by testing noble metal catalysts, i.e. Pt, Pd, Au, Rh, and metal oxide catalysts, such as Mn_2O_3, NiO, Cr_2O_3, V_2O_5, that dispersed on high surface area support materials, like Al_2O_3, SiO_2 and TiO_2 for catalytic VOC oxidation

(Spivey, 1987). Since methanol is a non-halogenated VOC, its oxidation is expected to reach higher conversions at lower temperatures on noble metal catalysts.

All of the studies that performed on catalytic VOC destruction show that, the hydrophobic catalysts are highly active for VOC oxidation at lower temperatures and show less susceptibility to water, which is a rate inhibitor for the active sites for the catalysts (Sharma et al., 1995).

In 2001, Badlani et al., was defined the methanol as a "smart" chemical probe. This is just because of the variable product distribution of methanol oxidation on different surface active sites existence on metal oxides. On redox sites formaldehyde (H_2CO) is primarily formed, also di-methyl ether (CH_3OCH_3) and carbon dioxide (CO_2) are generated on acidic sites and basic sites, respectively. This was the hint for the complexity of the methanol oxidation and the structure sensitivity of methanol (Badlani et al., 2001).

2.1.1. Metal Oxide and Metal Oxide Supported Catalysts

Metal oxide catalysts are usually consists of transition metal oxides, that is, between III-B and II-B. They have positive oxidation numbers and high electron mobility. In comparison to the metal oxide catalysts, supported noble metal catalysts are more active. However, metal oxide catalysts are more resistant to poisoning, which can be because of having higher active surface area rather than the supported noble metals. Metal oxides can be single or mixed due to the reaction (here is "oxidation") that is interested in. (Spivey, 1987) But, in literature these oxides are divided by the stability of the oxide as the most stable oxides, intermediate stable oxides and unstable oxides (Golodets, 1983). I-A and II-A groups metals (alkali and alkaline earth metals), the rare earth metals, the actinides, metals of the subgroups containing Sc, Ti, V, Cr and Mn, and Al, Zn, Sn, Ga, In, Ge form the most stable oxides (ΔH^o_{298} > 65 kcal/g-atom O). The metals that responsible for the forming of intermediate stable oxides (ΔH^o_{298} = 40 - 65 kcal/g-atom O) are transition metals and Cd, Sb, Pb, Bi, Tl. Finally, unstable oxides (ΔH^o_{298} < 40 kcal/g-atom O) are the noble metals, such as Pt, Pd, Rh, Ru, Ir, also Ag, Au and Hg (Golodets, 1983). This classification is useful to see that the unstable oxides can easily be reduced using a reducing agent, like hydrogen. On the other hand, as mentioned above SiO_2, TiO_2, ZrO_2, Al_2O_3, CeO_2, Nb_2O_5, MgO and La_2O_3 are the most

stable metal oxides (above 100 kcal/mole) and have high heat of formation, which make them usually applied as catalyst supports (Spivey et al., 2004).

Hinz and his coworkers were studied on the alumina supported platinum catalyst (Pt/Al_2O_3) with the contents of three different platinum loadings as 0.1, 1.0 and 3.0 wt%. Methanol oxidation was tested on these catalysts at lower temperatures in the absence and the presence of a trace amount of ammonia to reflect the industrial plants off-gas. Ammonia was found as the inhibitor in this study, too, like Ostermaier et al. and Luy et al (Ostermaier et al., 1976; Luy et al., 1984). In the absence of NH_3, high conversions to CO_2 observed with the 1.0 wt% Pt/Al_2O_3 which is close to the performance of 3.0 wt% Pt/Al_2O_3 and higher than the 0.1 wt% Pt/Al_2O_3 (Hinz et al., 2002).

Methanol oxidation reactions were performed over Pt nanoparticles supported on different metal oxide powder materials. The tests were done in two categories consisting of small (~8-9 nm) and large (~15-18 nm) platinum particles that deposited on CeO_2, TiO_2, SiO_2, ZrO_2 and Al_2O_3 support materials. All of the tested Pt/oxide-support catalysts were proceed through the direct oxidation of methanol. Pt/CeO_2 was more active between the large platinum nanoparticles, however, Pt/ZrO_2 was found as the most active catalyst among the smaller platinum particles. It was claimed that the electronic state of the support materials were affected by the surface Lewis acid sites. Also, this study shows that, the particle size, oxidation state of O_2 and choice of the support are important parameters for this type of reaction (Croy et al., 2007).

Transition metals, like Cr, V, Mo, W, Mn, Zn, Fe, Re and Sn, Ga, In and Ge sp-metals that show intermediate stability of their oxides are usually used as promoters in supported metal catalysts (Spivey et al., 2004). Chantaravitoon and coworkers were studied combustion of methanol over the monometallic platinum and bimetallic platinum-stannum on alumina support between the temperature ranges of 35-300^oC. Excess oxygen (21% O_2) was used in the reactions where methanol was in the range of 500-1200 ppm. Throughout the study, alumina supported monometallic Pt catalysts activity was found higher than the bimetallic Pt-Sn on alumina catalysts. Increasing tin content leads to the shifting of the overall conversion to higher temperatures. Instead of promotion, adding tin causes to the deactivation of the Pt/Al_2O_3. The main carbon containing products of methanol combustion for both types of the catalysts were CO_2 and methyl formate (CH_3OCHO) (Chantaravitoon et al., 2004).

Another study similar to the Chantaravitoon and coworkers were performed by Arnby et al., with adding magnesium over the Pt/Al_2O_3 catalysts. The catalysts were prepared by wet-impregnation method. The precursor sources were platinum nitrate and magnesium nitrate solutions that led to the $MgAl_2O_4$ spinel and MgO were formation over the Pt/Al_2O_3 catalysts. Testing of catalysts were performed on methanol and carbon monoxide oxidation in the presence of ammonia. The object of adding magnesium over the Pt/Al_2O_3 catalysts were to improve the low temperature activity and lower the inhibition effect of the ammonia. However, addition of increasing amount of magnesium led to the blocking of surface active sites and caused to substantial decrement of platinum dispersion on the supported material. Therefore, low temperature activity for methanol oxidation was decreased in comparison to the undoped Pt/Al_2O_3 catalysts (Arnby et al., 2004).

Álvarez-Galván and coworkers were studied with the alumina supported manganese catalysts with variable manganese loadings ranging between 3.9 to 18.2wt%. The catalysts testing were performed in the combustion of formaldehyde/methanol mixture in air. The higher the manganese loading resulted with the higher activity. Complete combustion temperature of 18.2% Mn/Al_2O_3 catalyst was 220^oC showed decrement in the complete combustion temperature as 90^oC when 0.1% Pd was incorporated to the alumina supported manganese catalyst. Addition of small amounts of palladium metal into the Mn/Al_2O_3 improved the activity of the highest Mn-loading (18.2% Mn/Al_2O_3) catalyst. The characterization of the catalysts were showed that the MnO_2 and Mn_2O_3 phases are exist on the surface of the catalyst and oxidation ability of these phases are determined the activity of the catalyst. In addition to that, higher activity of the $Pd\text{-}Mn/Al_2O_3$ catalysts than the Pd/Al_2O_3 catalysts were concluded that PdO_x moiety and also $PdO_x\text{-}MnO_x$ interaction are responsible in the oxidation reactions (Álvarez-Galván et al., 2004).

Al_2O_3 supported Cu, Au and Ag catalysts and the addition of CeO_x and Li_2O to the $Metal/Al_2O_3$ catalysts effect were investigated in methanol oxidation by Lippits et al. Cu/Al_2O_3 catalysts were found as the most active catalyst in the methanol oxidation and were the most selective catalyst to CO_2 formation. Silver particles were observed as the responsible metal for partial oxidation of methanol. Also gold particles were showed similar behavior as having selectivity to the partial oxidation of methanol. CeO_x addition led to the increment to the CO and CO_2 selectivity which was acted as a co-catalyst next to the dispersed metal particles. However, Li_2O was observed as the

blocking agent of the adsorption site on alumina and hence, led to the decrement of the formaldehyde product (Lippits et al., 2009).

Different support and metal, co-precipitated Au/Fe_2O_3, was studied by Minicò and coworkers in combustion of volatile organic compounds with excess amount of oxygen. Increasing amount of gold content in the catalysts result with the decrement of the total combustion temperature (light-off temperature) that explains the gold particles high catalytic activity. Throughout the experiments, for undoped Fe_2O_3 catalyst, the oxidation was begun at 180^oC and complete oxidation was achieved above 270^oC. However, for the gold dispersed Al_2O_3 catalyst, the start-up temperature of the oxidation was about 80^oC and the total oxidation was observed at 160^oC. It was asserted that the highly dispersed gold particles are responsible to decrease the strength of the Fe-O bond that results with the improving the mobility of the lattice oxygen which participates in the oxidation of volatile organic compounds (Minicò et al., 2000).

2.1.2. Noble Metal Catalysts

Even though, the most generally used catalysts for oxidation/combustion of volatile organic compounds are metal oxide supported noble metals, unsupported or non-metal oxide supported noble metals also are investigated previously and have been used in some practical systems (Spivey, 1987; Sharma et al., 1995; Xu et al., 2008; Ferrin et al., 2009). Especially platinum, palladium and a few alloys are led in this way. The reason of why these are the most favorable catalysts is the ability of operating at high temperature required systems, i.e. catalytic incineration and automotive exhaust catalysts. The other metals may undergo sintering, volatility loss and irreversible oxidation at high temperatures (Prasad et al., 1984; Spivey et al., 2004).

Spivey et al., in 1987, was also mentioned about the high catalytic activity for oxidation at low temperatures and high selectivity of the noble metal catalysts for the complete oxidation products, namely carbon dioxide and water. On the other hand, deactivation tendency of the noble metals by poisoning, especially by halogenated compounds, limited supply and the high cost of the metals cannot be underestimated (Spivey et al., 1987).

Sharma and colleagues were investigated the activities of fluorinated carbon supported Pt, Pd, and Pt-Pd catalysts. Although Cordonna et al. were observed and

increment in hydrocarbon conversion with increasing amount of metal loading, Sharma and co-workers were not found an increment for methanol destruction with increasing metal loading. Until the temperatures of 100-110^{o}C, Pt loaded catalysts and bimetallic Pt-Pd doped catalysts have resulted with the same conversion, after around 110^{o}C even if a decrement was observed for supported monometallic Pt catalysts, supported bimetallic Pt-Pd catalysts were showed higher conversion. Monometallic palladium catalysts were indicated the lowest conversion in all of them (Sharma et al., 1995). The higher activity of the Pt catalysts compared to the Pd catalysts were grounded to the strong adsorption of oxygen on platinum (Spivey, 1987). In addition to this study, similarly, Hicks et al. were found Pt catalysts more active than the Pd catalysts in the oxidation of n-heptane and Cordonna and coworkers were also observed that, the Pt catalysts are much higher active than the Pd catalysts in carbon monoxide oxidation (Hicks et al., 1990; Cordonna et al., 1989).

In the manner of sustainable energy, a few different types of nanocatalysts were covered as can be used in electrooxidation. Xu research group was studied with the Pt-Ru nanocomposites, gold nanocatalysts, and carbon nanotubes supported Pt-Fe catalysts. Using Pt-Ru/vulcan carbon powder nanocomposites as anode catalysts for DMFC were essentially increased the cell performance than commercial, unsupported Pt-Ru colloidal catalysts. Also, it was referred that silica supported Pt catalysts were generated higher initial current density for methanol oxidation than commercial Pt/C catalysts (Xu et al., 2008).

If we consider all of the studies done about the catalytic oxidation of methanol over the metal oxide catalysts (supported/unsupported) and noble metal catalysts (supported/unsupported), it can be clearly said that Lewis acidity plays a crucial role in modifying the reactions and also in determining the reaction pathways that will be proceeded since the adsorption tendency of the reactant species are dependent on both the electronic state and the stability of the supported materials.

2.2. Product Distribution of Methanol Oxidation on Different Catalysts

The product distribution can change with the mechanism that the reaction follows. In the presence of oxygen volatile organic compounds can follow four possible reaction pathways to form different species. For the case of methanol, it can be go to

complete combustion (total oxidation), incomplete combustion, partial oxidation and oxidative dehydrogenation. Mostly, these reactions are divided into two groups as complete oxidation and partial (selective) oxidation. Since the reaction occurs on the surface of the catalysts, the interaction between the metal and the oxygen are important. Weak metal-oxygen bonds are required for catalysts to completely oxidize the reactants (Simons et al., 1968; Boreskov et al., 1971). Haber and coworkers were referred that "surface adsorbed" oxygen may led to the total oxidation, while for partial oxidation lattice oxygen is required (Haber, 1975).

Sharma et al. were found that the fluorinated carbon supported Pt, Pd and bimetallic Pt-Pd catalysts that studied within the temperature range of 50 and 400^{o}C. Oxygen amount was much higher than the VOC concentration, therefore they assumed that the reaction proceeded to the complete oxidation over intermediate formation, and the only carbonaceous product is CO_2 (Sharma et al., 1995).

Badlani research group were investigated the methanol combustion product distribution. They asserted that these reactions were projected the character of the surface active sites on different metal oxide catalysts. Also, they observed that the metal oxides redox sites were generated formaldehyde, acidic sites were yielded di-methyl ether and basic sites were produced CO_2. Throughout the study, CeO_2, CaO, CuO, La_2O3, PdO, TeO_2, Au_2O_3, SnO_2, Sb_2O_3 and Ag_2O were given 100% selectivity to formaldehyde; acidic products were formed with 100% selectivity by Nb_2O_5, Al_2O_3, P_2O_5; CO2 was the only product of Y_2O_3 and In_2O_3. ZrO_2, Co_3O_4, BaO, MgO, SrO, Mn_2O_3 and NiO were found more selective to formaldehyde but less selective CO_2, whereas PtO, Rh_2O_3, ZnO and Cr_2O_3 were found more selective to CO_2 but less selective to formaldehyde (Badlani et al., 2001).

Another study's temperature programmed desorption (TPD) results showed that, on both Al_2O_3 (Hinz et al., 2001; Cordi et al., 1996) and Pt/Al_2O_3 (Hinz et al., 2001; Imamura et al., 1999) methanol oxidation products are H_2, CO, di-methyl ether, CO_2 and also consistent with the previous studies. Over unsupported Pt, destruction of methanol was primarily yielded hydrogen and carbon monoxide (Sexton et al., 1921; Kizhakevariam et al., 1993). If any oxygen exists on the surface, CO_2 (Kizhakevariam et al., 1993) and formaldehyde (Wang et al., 1994) may be yielded as well. In addition to that, in the same study it was observed that for low amount of Pt in Pt/Al_2O_3 formation of dimethyl ether and formaldehyde were high whereas for high amount of Pt in Pt/Al_2O_3 formation of CO, H_2 and CO_2 were high (Hinz et al., 2002).

Croy and coworkers were studied with different metal oxide supported Pt doped catalysts. For pure metal oxides (support materials) the reaction was carried out at the temperatures of 150^{o}C, 200^{o}C, 250^{o}C and 300^{o}C. Pure alumina was not active at the temperature of 150^{o}C, but showed selectivity to produce dimethyl ether even at 300^{o}C. It was observed that Pt/Al_2O_3 was behaved similar to Pt/TiO_2 catalysts below 200^{o}C, but after 200^{o}C Pt/Al_2O_3 was slightly more active than Pt/TiO_2 (Croy et al., 2007).

Chantaravitoon and colleagues were studied the oxidation of methanol in the presence of excess oxygen (21%) with changing methanol concentrations between 500-1200ppm and in the temperature range of 35-300^{o}C over the Pt and Pt-Sn alumina supported catalysts. They observed that CO_2 and methyl formate were the only carbonaceous products of methanol oxidation. Methyl formate was formed higher at low temperatures whereas CO_2 was yielded higher at high temperatures (Chantaravitoon et al., 2004). These results were found as in good agreement with the other studies results reported by McCabe and Mitchell (McCabe et al., 1986). They also found that CO_2, methyl formate and formaldehyde were the only carbonaceous products in methanol oxidation over alumina supported Pd, Pt, Rh, Ag and Cu-Cr catalysts.

Thompson and Bond were explained that gold and platinum catalysts in oxidation of methanol proceed on different reaction pathways. Using platinum as a catalyst was yielded firstly with carbon monoxide and then carbon monoxide was oxidized to carbon dioxide. However, using gold as a catalyst was firstly resulted with the formaldehyde formation, after that formaldehyde was oxidized to carbon dioxide (Thompson et al., 1999). Minicò et al. were investigated the methanol oxidation on Au/Fe_2O_3 catalysts and they have found that no partial oxidation product formation, carbon monoxide was the only carbon containing product in the reaction (Minicò et al., 2000). On the other hand, Lippits research group were studied with the Al_2O_3 supported Cu, Au and Ag catalysts and were observed that Au/Al_2O_3 catalysts cannot completely oxidized. They suggested a possible mechanism for methanol oxidation, which is firstly methanol decomposes to formaldehyde on the Al_2O_3 support at low temperatures, then with the increase of the temperature formaldehyde oxidizes to carbon monoxide on gold. Gold was claimed as selective to CO formation at high temperatures (Lippits et al., 2009).

Different metal oxide and noble metal catalysts were tested to find the best catalytic performance and to understand the mechanism of the catalytic oxidation of methanol. Selectivity to partial or complete oxidation was found to be changing with

respect to the metal and the support material. Platinum was showed the best catalytic activity in all studies and aluminum oxide was found to be selective to produce CO_2. On the other hand, only one in literature was focused on the methanol oxidation over Pt/Al_2O_3 below room temperatures but, in literature the product distribution of the methanol oxidation was not studied before (Dönmez, 2011). Therefore, this thesis is focused on investigating the product distribution of the methanol oxidation at room temperature and also below room temperatures.

CHAPTER 3

MATERIALS AND METHOD

3.1. Materials and Equipment

In this study, alumina (Al_2O_3) and alumina supported platinum catalyst (Pt/Al_2O_3) were synthesized with the loading of 2wt.%Pt. In preparing the catalysts, aluminum isopropoxide (AIP, Alfa Aesar) was used as a precursor whereas nitric acid (HNO_3, Merck) was used as the peptizing agent. Al_2O_3 powders were synthesized with the modified single step sol-gel method (Donmez, 2011). Besides pure Al_2O_3 synthesis, alumina supported platinum doped powders were prepared by wet-impregnation method. The chemicals used in the synthesis of the catalysts were listed below in Table 3.1.

Table 3.1 Properties of chemicals used in catalyst synthesis.

	Chemical formula	Molecular Weight	Purity (%)
Aluminum Isopropoxide	$Al[OCH(CH3)_2]_3$	204.24	98
Platinic Acid	$H_2PtCl_6.6H2O$	517.91	99.9
Nitric Acid	HNO_3	63.01	65

3.2. Methods

Throughout this work, the experiments can be categorized into three groups;

- Catalyst preparation
- Catalyst characterization
- Catalytic oxidation of methanol

3.2.1. Catalyst Preparation

3.2.1.1. Preparation of Alumina Supported Platinum Catalysts

Aluminum oxide and aluminum oxide supported platinum catalysts were synthesized and used in a fixed bed micro-reactor in catalytic methanol oxidation. During the synthesis, a modified single step sol-gel method was followed. First step of preparing alumina support materials was the hydrolysis of AIP. Deionized water and AIP were mixed together to lead the hydrolysis reaction in the concentration of 0.1 g/mL (AIP/water) at 85^{o}C and stirred for 1 hour. In the second step adding HNO_3 to this solution caused the peptization reaction at the same temperature and mixing time. At the end of this step, sol was obtained. Then, the sol was kept at around the same temperature to form the gel. After gelation, the catalyst was dried at 120^{o}C overnight and then, calcined at 500^{o}C for 6 hours. After finalization of calcination, alumina catalysts were sieved to 60mesh (250 μm) before the impregnation.

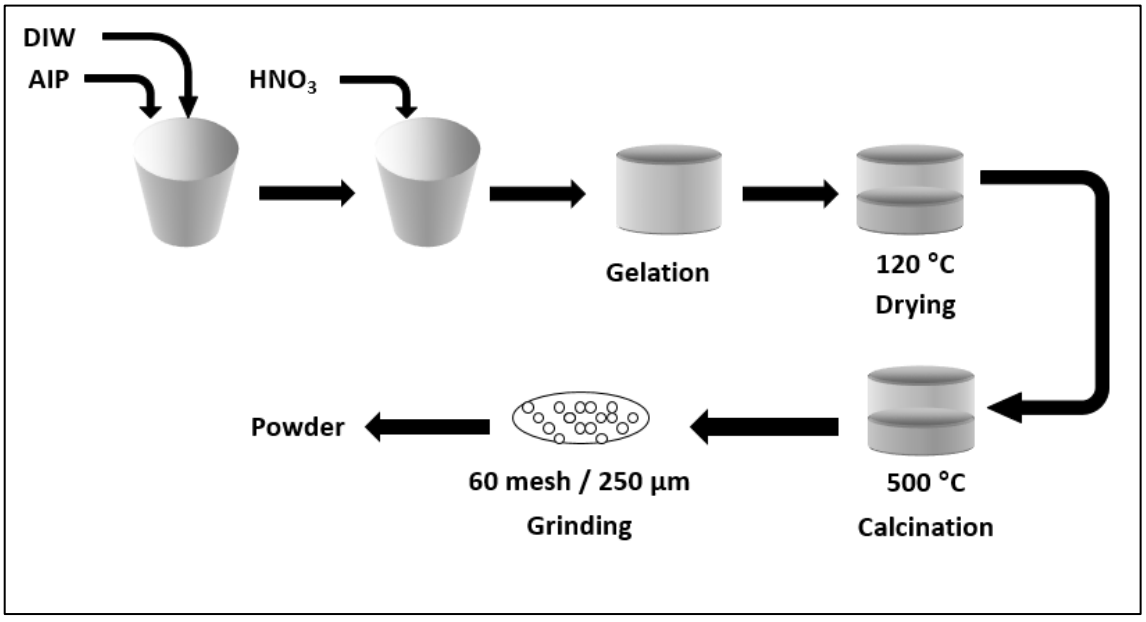

Figure 3.1 Preparation of alumina powder catalysts

To prepare the platinum dispersed alumina supported catalysts as mentioned earlier, incipient wetness impregnation method was used. In this procedure, first the

pore volume of the alumina was found and then, required platinum precursor was weighed for 2wt.% Pt/Al_2O_3. Finally, platinum precursor solution was added to the alumina support. After that, the catalyst was dried at 120^oC in an oven for overnight, which followed by calcination at 500^oC for 6 hours.

3.2.2. Catalyst Characterization

In the characterization of the samples BET analysis (N_2 adsorption) and X-Ray Diffraction (XRD) techniques were used.

3.2.2.1. Textural Properties

BET analysis was used to find the porosity, total surface areas, average pore diameters and pore distributions of the catalysts. The measurements were performed by Micrometrics ASAP 2010 by N2 adsorption at 77.34 K. The calcined catalysts were dried at 120^oC overnight before the analysis.

3.2.2.2. X-Ray Diffraction (XRD)

Philips Xpert XRA-480 Model X-Ray diffractometer was used to identify the XRD pattern of the catalysts. Crystalline structures existence were evaluated by the analyzed XRD patterns.

3.2.3. Catalytic Oxidation of Methanol

The fixed bed reactor set-up where catalytic oxidation of methanol was performed over the Pt/Al_2O_3 is shown in Figure 3.2.

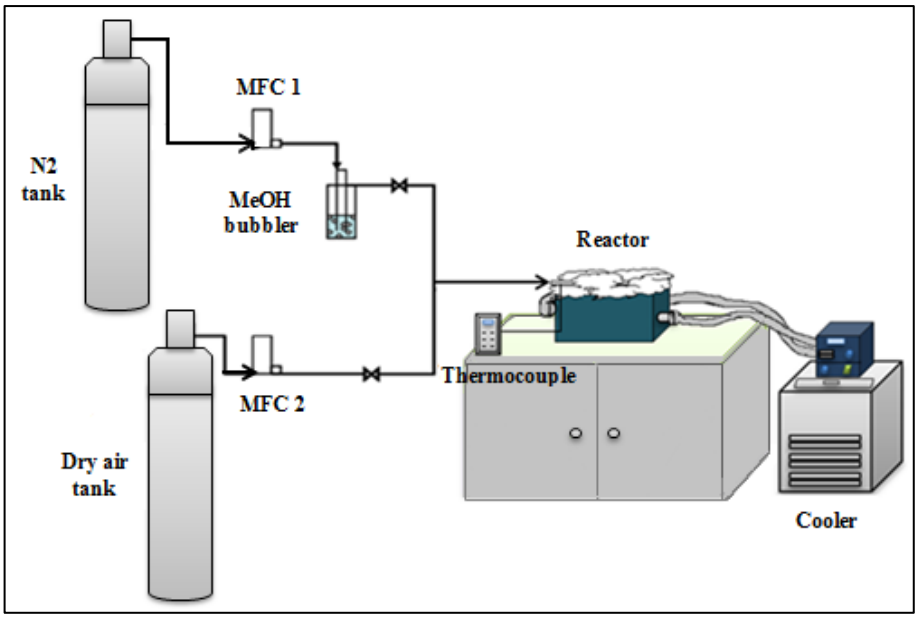

Figure 3.2. Reactor set-up for catalytic methanol oxidation

Methanol was placed in a well-sealed glass bubbler and helium was sent to the bubbler in order to vaporize methanol. Helium also plays a role as a carrier gas. Dry air, which was used as oxygen source, was mixed with helium and methanol vapor and this gas mixture was sent to the reactor. The reactor size was 10 mm ID., 16.4 mm OD. and 152.4 mm in length. The catalyst was placed between two glass wool stoppers.

Brooks Instrument 5850 model mass flow controllers were used to adjust the concentration of dry air and helium and they were represented in the figure as MFC1 and MFC2. Reaction temperature on the reactor surface was measured with a K-type thermocouple and the data were recorded. To be analyzed by gas-chromatography instrument, gas samples were collected using glass gas sampling bulbs.

Catalytic activity was performed after the platinum doped alumina supported catalyst was activated. For this purpose, the catalyst was put in an oven at 400^{o}C for two hours to get rid of the adsorbed species, such as water or carbon dioxide. After that, the catalysts were washed with methanol to be activated and methanol was drained by dry air for a few seconds. Lastly, drained catalyst was dried at 120^{o}C for one hour and it was ready to be used in the reaction.

The inlet reaction temperature was changed from -13^{o}C to 28^{o}C to understand the behavior, such as the product distribution, of methanol combustion over Pt/Al_2O_3 catalysts.

CHAPTER 4

RESULTS AND DISCUSSION

4.1. Combustion of Methanol

The activities of aluminum oxide supported monometallic Pt loaded catalysts were tested in oxidation of methanol in a packed bed tubular reactor at room and below room temperatures. From the literature, it is known that the aluminum oxide supported platinum catalysts are very selective to carbon dioxide formation during the catalytic combustion of methanol. Since the total combustion products of the reactions are CO_2 and water, measuring the reactor temperature was thought to be used as a reference for us to indicate the conversion of the reaction. For this reason, adiabatic flame temperature calculation was used to help us in making better comparison of the catalysts at different space velocities and varying temperatures. The calculations are given in Appendix A.

During the reactions, the temperature change throughout the day, and opening windows to provide the ventilation in laboratory caused the temperature fluctuations which then was chain-effected the flow rate fluctuations. For this reason, the inlet methanol concentration fluctuated between 0.30% and 0.39% methanol in air.

Before carrying out the reaction an activation procedure was applied to remove the chlorides, which is responsible for deactivation of the catalysts. In addition to that, this procedure was conducted to reduce the calcined catalyst from PtO_x active sites to Pt crystallites sites. In this activation, around 5 ml of methanol was drained by air from the catalyst that will be used in the reaction and dried in an oven around 1 hour at 120^{o}C.

In methanol combustion, platinum catalysts show higher activity and compared to the other catalysts, the platinum catalysts are known to less prone to the deactivation. The reactions in this study were done by the fresh catalysts in order to have a better opinion about the product distribution of the Pt/Al_2O_3 catalyst at different initial temperatures and residence times.

During the reaction, it was important to have reaction conditions free of the internal and external mass transfer limitations. Since, the reactor inner diameter is 1 cm,

the catalyst particle size less than 250μm would be enough to avoid excessive pressure drop and also, to eliminate the internal mass transfer limitation. That's why the catalyst particles were sieved below 250μm. To avoid the external mass transfer limitation, the film thickness around the catalyst particles must be decreased with increasing flow rate. Schiffimo and colleagues reported in 1993, 50 ml/min flow rate was enough to be free of the external mass transfer limitation. In addition to that, another study was practiced recently by our research group on methanol combustion with almost the same conditions with our reaction parameters and it is proved that 50 ml/min flow rate is sufficient to eliminate the mass transfer limitation (Dönmez, 2011). For this reason, the activity of the catalysts was tested in this study at 50 ml/min total flow rate.

Previous work conducted by our group showed that the time to reach the temperature of DMFC operation and the steady state temperature was resulted in higher activity with the loadings of 2% and 5% Pt (Dönmez, 2011). Since, the price of platinum is high, the 2% Pt/Al_2O_3 catalyst was decided to be used in this study.

4.2. Space Velocity and Initial Temperature Effect on Combustion of Methanol

One of the important parameters in reaction engineering is the contact time of the catalysts with the reactants. In that manner, residence times, that are the reciprocal of space velocities, are important parameter on catalytic activity of the reactions. The product distribution or conversion can be controlled by changing space velocity. Three different space velocities, 2.4 s^{-1}, 2.8 s^{-1} and 3.1 s^{-1}, were used in this thesis on fresh 2% Pt/Al_2O_3 catalyst. The ratio of the total feed volumetric flow rate (at 25^{o}C and 1 atm) to the catalyst volume is defined as the "space velocity".

It is expected that, with increasing space velocities, that is, decreasing the contact time of the catalysts with the reactants may reduce the activity of the catalysts. This can be because of the different intermediates formation that negatively affects the surface active sites. This negative effect may be due to the active site blocking during the reaction by the formed "undesirable" intermediate species, which would change the reaction pathway.

Figure 4.1 indicates the effect of space velocity on methanol combustion over 2% Pt/Al_2O_3 catalysts. The average temperature was found as 120°C, 123°C and 112°C for 2.4 s^{-1}, 2.8 s^{-1} and 3.1 s^{-1} space velocities, respectively.

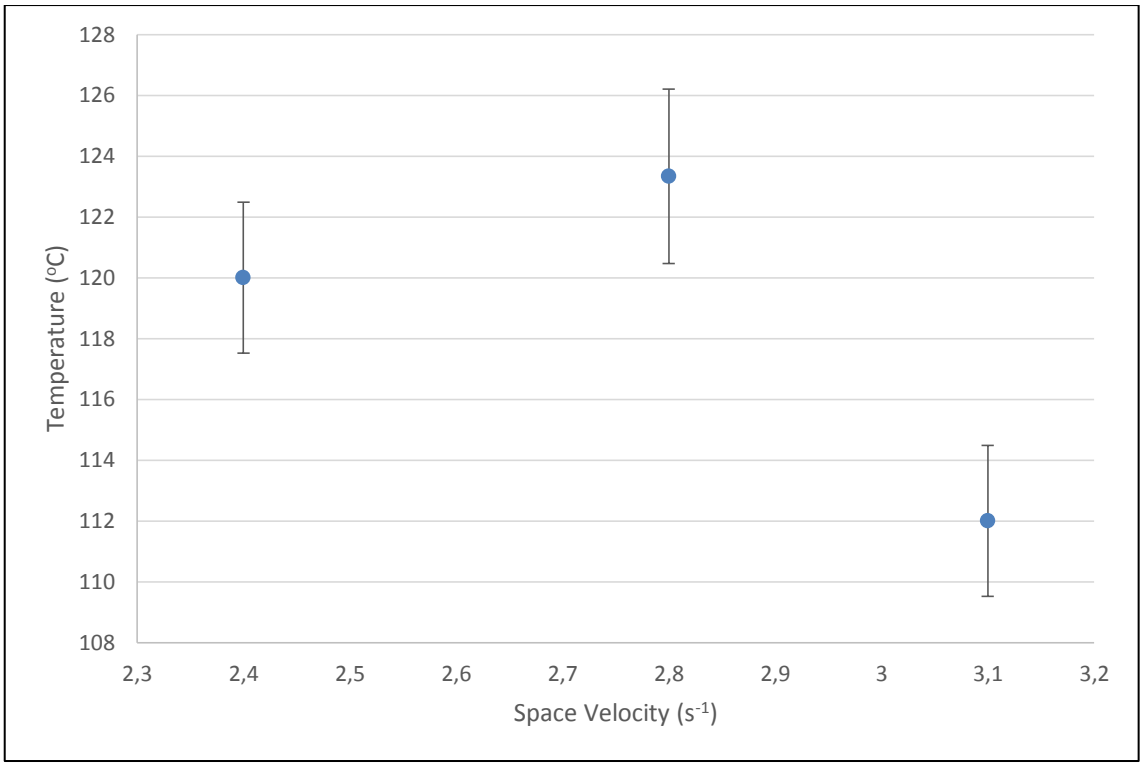

Figure 4.1. Temperature vs Space Velocity for 28°C.

It is known that in packed bed reactors, with increasing space velocity, conversion must be decreased. To see whether if the product distribution changes or not with changing space velocities, three different space velocities with 15% increment were tested. However, as can be seen in figure 4.1, for 2.4 s^{-1} and 2.8 s^{-1} space velocities error bars are overlapping. Therefore, it can be said that 2.4 s^{-1} and 2.8 s^{-1} has almost the same activity and increment of 15% of space velocity is not enough to see the effect. On the other hand, 3.1 s^{-1} has lower steady state temperature and its error bar is not overlapping with the others.

To better see the effect of the space velocities on the product distribution, GC-TCD and GC-MS analysis was conducted. GC-TCD analysis was used to detect the CO or CO_2 gases whereas GC-MS was used to analyze the unknown gas species. During the

GC-TCD analysis no CO peak was observed, so that all of the GC-TCD figures below only represents the conversion to CO_2.

The samples were collected at three different parts of the S-shape of the temperature vs. time graph. First of all, when the reaction was begun, the gas sample was started to be collected and this part was named as “start-up part” and indicated as “1” in Figure 4.2. When the reaction was reached 35^{o}C, where the fast exponential increment was observed, and gas sample was collected, but this part was called as “increment part” and indicated as “2” in Figure 4.2. Lastly, when the reaction temperature reached at a steady state temperature, the gas samples were collected two or three times with 10 minutes intervals to better show the reaction reached steady state. These parts were named as “steady parts” and indicated as “3-1”, “3-2” and “3-3” in Figure 4.2.

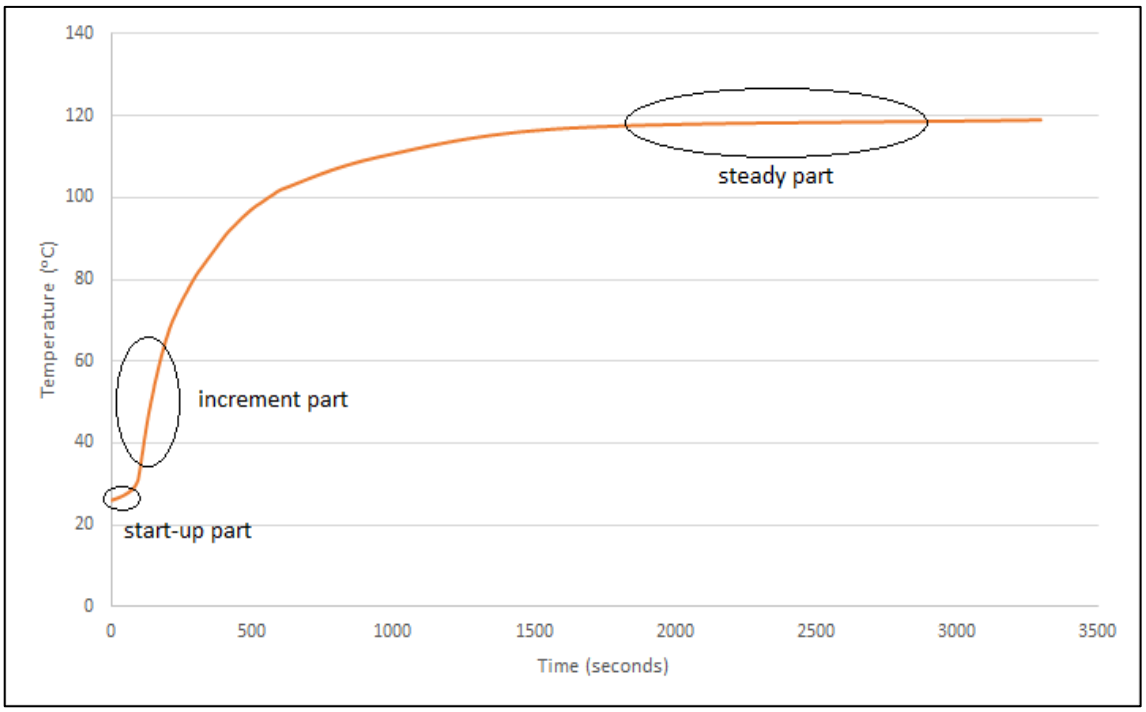

Figure 4.2. Temperature vs time (S-Shape behavior).

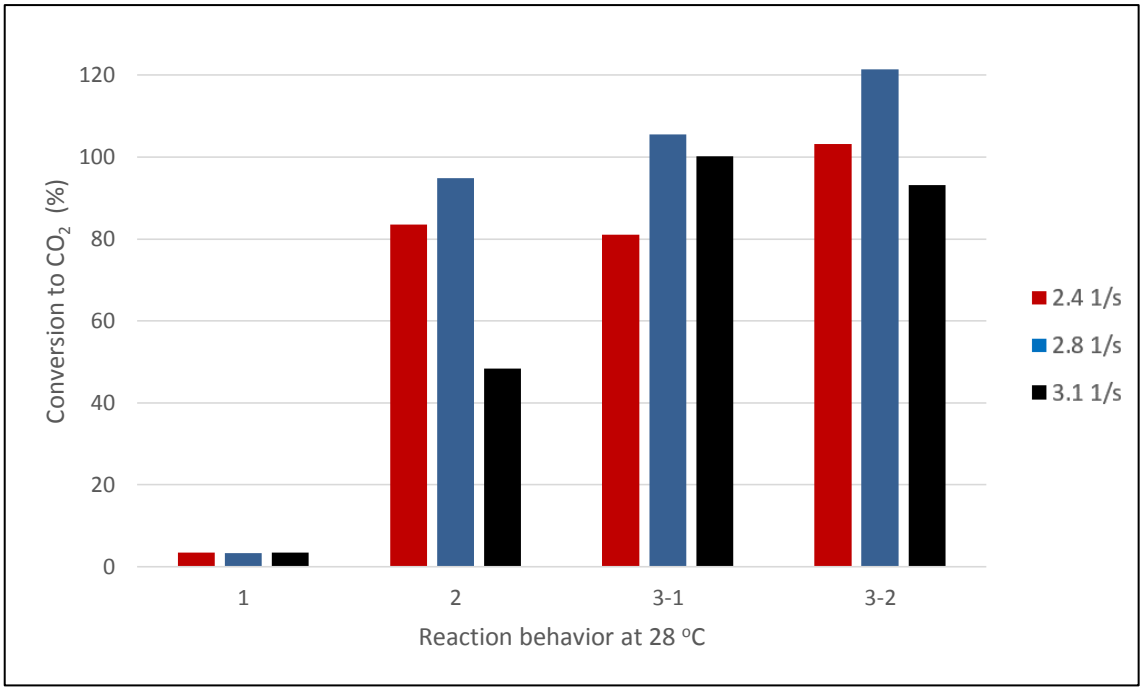

Figure 4.3. Conversion to CO_2 at 28°C of inlet temperature for all the space velocities.

The maximum steady state temperatures reached with the oxidation of methanol at 28°C was found to be 117°C, 120°C and 113°C for the space velocities of 2.4 s^{-1}, 2.8 s^{-1} and 3.1 s^{-1}, respectively. With the decreasing residence time, the surface coverage decreases; thus, the catalytic activity reduces and product distribution may be affected with changing space velocities (Silva, 2007). To investigate this fact, GC-TCD and GC-MS analyses were carried out.

Adiabatic flame temperature calculations must be covered with the observed maximum steady state temperatures. In Table 4.1, some information about the conditions and observed maximum temperature, theoretical maximum temperature (maximum adiabatic flame temperature) were given. Observed maximum temperatures for 2.4 s^{-1} and 3.1 s^{-1} are consistent with each other. However, since observed maximum temperatures can't be higher than the theoretical maximum temperatures, there is an unexpected behavior in 2.8 s^{-1} data. The observed maximum temperature is 10°C higher than the theoretical maximum temperature. This could be because of the temperature fluctuations during the day which can be led to the increment of the inlet methanol concentration and resulted with the observed maximum temperature increment.

Table 4.1. Conditions and calculations for 28^{o}C inlet temperature activity tests.

	2.4 s^{-1}	***2.8 s^{-1}***	***3.1 s^{-1}***
Methanol Mole Amount	3340 ppm	3074 ppm	3317 ppm
Observed Max. Temp.	117 ^{o}C	120 ^{o}C	113 ^{o}C
Theoretical Max. Temp	118 ^{o}C	110 ^{o}C	118 ^{o}C
Theoretical Max Conversion	~100%	~100%	~100%

It can clearly be seen from Figure 4.3 that, the conversion to CO_2 at room temperature is showed an increment with increasing time. At start-up part, the conversion for three different space velocities were almost the same and low, around 2-3%. When we look at the increment part 2, 2.4 s^{-1} and 2-8 s^{-1} are over 80% conversion, but 3.1 s^{-1} is around 50%. When the temperature started not to change more than 1-2^{o}C, the steady part gas samples were collected. At room temperature, the reactions were come to the steady state around 25th minute. However, the samples were collected at 50th and 60th to be completely sure the reactions are at steady state. Figure 4.3 shows the conversion to CO_2 for 2.4 s^{-1} and 3.1 s^{-1} space velocities are around 100%. However, it can be seen from the figure that, for the 2.8 s^{-1} space velocity, the CO_2 conversion goes to the 120%. This is not possible to find it more than 110% even within the 10% experimental error. There can be two possibilities, either the temperature is increased during the reaction and caused increment of the methanol amount that sent to the reactor, which is consistent with the Table 4.1, or during collecting and transferring the gases between the tubes and vials, concentration (pressure) difference can be caused this. That's why 2.8 s^{-1} space velocities theoretical conversion was evaluated as 100%. There are some inconsistencies with the steady state gas analysis at 3-1 and 3-2 sampled gases. These inconsistencies are again because of the sampling and transferring the gases between tubes and vials. To have an opinion about the uncertainty, these analysis must be repeated between 3 or 5 times or an online GC apparatus would give more consistent data. Overall, it can be said that clearly with GC-TCD data, for all space velocities, the reaction goes to complete conversion within the error.

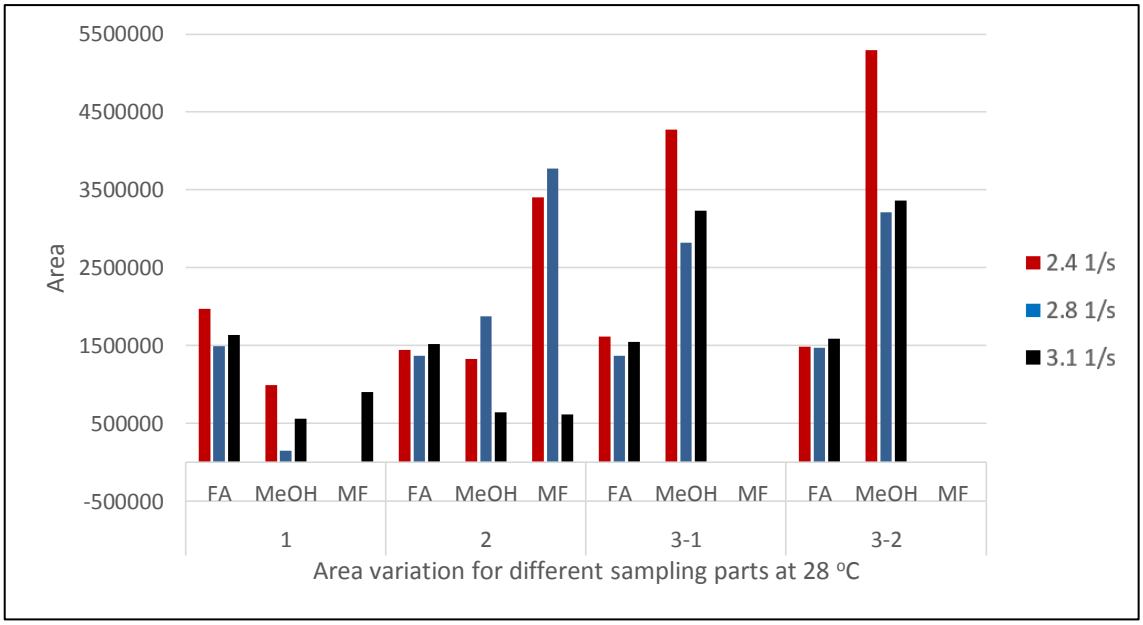

Figure 4.4. GC-MS Reaction behavior at 28°C inlet temperature.

GC-MS analysis was performed to determine whether if any other species (toxic gases, intermediates, etc.) formed or not for the same parts of the figure 4.2. In Figure 4.4, formaldehyde is indicated as "FA", methanol is indicated as "MeOH" and methyl formate is specified as "MF". Due to the lack of some chemicals, amount analysis could not be conducted by GC-MS data. However, area comparison is chosen to be mentioned to give an opinion about the species that formed and consumed during the reaction. For room temperature experiments (28°C) formaldehyde amount does not changed too much from beginning to the end and this trend is can be seen in other inlet temperature reactions below, too. Most probably this formaldehyde peak comes from the methanol that we used in this study. Methyl formate is found mostly at the increment part of the samples whereas there were not any for steady parts. Methanol peaks exist at the end of the reaction, since methanol is soluble in water and since one of the combustion product is water, methanol can be absorbed by little water droplets or adsorbed somewhere and then the release of this methanol may be led to these peaks, too. It can be seen at the steady part methanol peaks for three different space velocities exist. Since TCD results showed around 100% conversion for all space velocities. This situation is not expected throughout the analysis. As mentioned just above, maybe somehow the methanol vapor was absorbed by the condensed water droplets and then with the continuous flow they were released and gave that behavior. In addition to that, since an amount analysis could

not be performed, these peaks can belong to very low amounts of methanol, too. This is also acceptable for the other species.

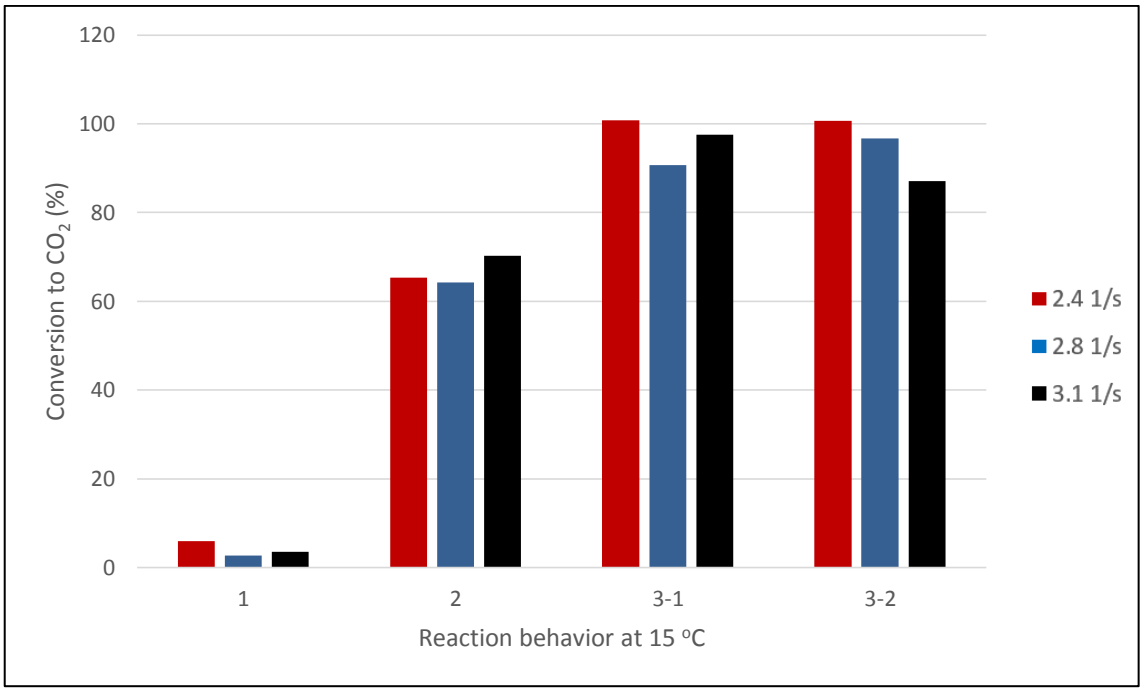

Figure 4.5. Conversion to CO_2 at 15°C of inlet temperature for all the space velocities.

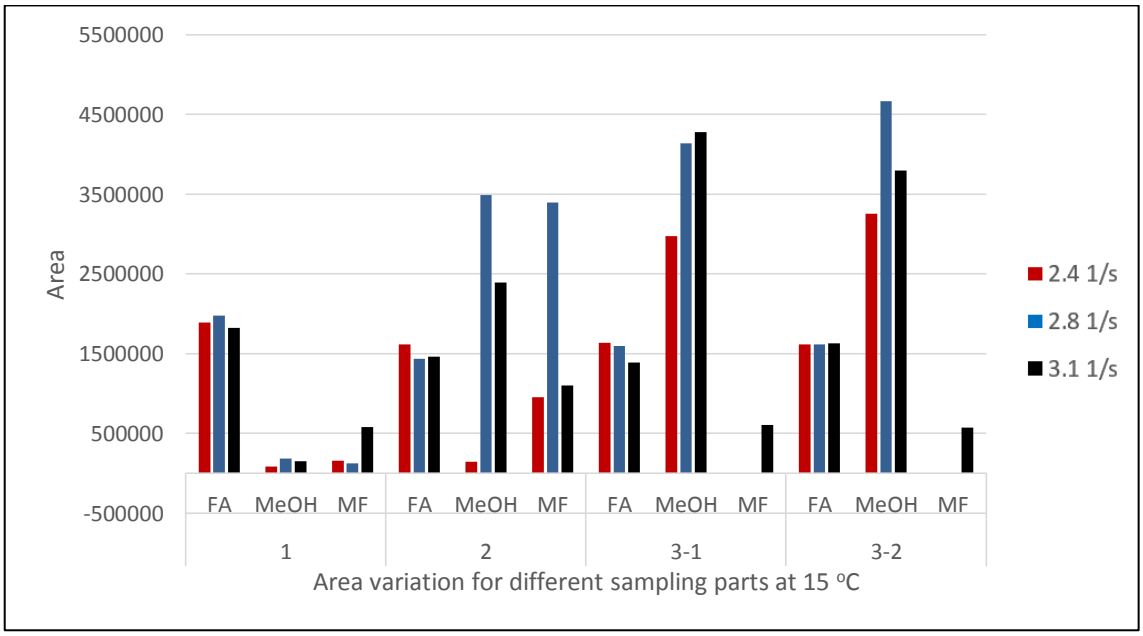

Figure 4.6. GC-MS Reaction behavior at 15°C inlet temperature.

Figure 4.5 gives the analysis results of CO_2 conversion at sub-room temperature (15^oC) for three different space velocities. Adiabatic flame temperature calculations help us again to find the theoretical conversion with respect to the methanol inlet mole amount. Table 4.2 shows the conditions and theoretical conversions again for 15^oC inlet temperature reactions. It can be seen from the table 4.2, all of the space velocities conversion are around 90%. Normally, since to see the effect of the space velocity is not enough for 15% increment as in the figure 4.1, for 2.4 s^{-1} and 3.1 s^{-1} a difference is expected. However, all of the space velocities theoretical reached conversions are around 90%. This can be because of the different intermediates formation and changing the pathway of the reaction with changing space velocities. When we look at the figure 4.5, it can be seen that all of the space velocities at sub-room inlet temperature tests are reached around 100% conversion again. Since GC-TCD results only reflects the conversion to CO_2, it can be said that with decreasing temperature, condensation of water droplets increases and the solubility of CO_2 in water increases, so that the analysis results could give us higher conversion to CO_2 if somehow the dissolved CO_2 is released to the gas sampling tubes during the reaction. In addition to that, methanol inlet amount fluctuation can be caused to this.

Table 4.2. Conditions and calculations for 15^oC inlet temperature activity tests.

	2.4 s^{-1}	***2.8 s^{-1}***	***3.1 s^{-1}***
Methanol Mole Amount	3396 ppm	3928 ppm	3905 ppm
Observed Max. Temp.	96 ^oC	111 ^oC	110 ^oC
Theoretical Max. Temp	106 ^oC	120 ^oC	120 ^oC
Theoretical Max. Conversion	~100%	~100%	~100%

In the figure 4.6, methanol peaks were observed at the steady parts, like in the 28^oC experiments. The same speculation may be done as in the case of the 28^oC experiments for the presence of methanol. Formaldehyde, which is coming from the methanol stock, again is not reacting and its area (amount) stays constant. Methyl formate takes part especially in increment part again, and since we reached the same trend in room temp tests, it could be said that the reaction most probably proceeds over methyl formate intermediate. Differently this time for 3.1 s^{-1} space velocity a little MF

peak is observed at steady part. However, since the calibration could not be performed and since this peak area is small it can belong to trace amount of methyl formate.

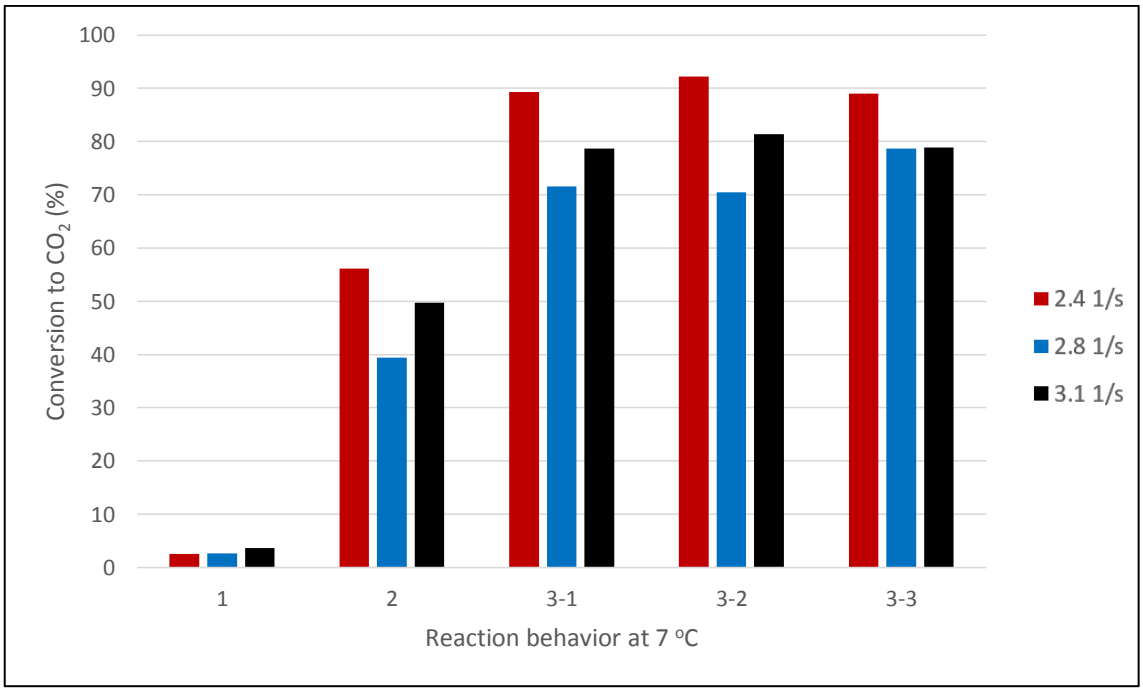

Figure 4.7. Conversion to CO_2 at 7°C of inlet temperature for all the space velocities.

It can be seen in the figure above, conversion to carbon dioxide at 7°C inlet temperature tests, for the space velocities of 2.8 s^{-1} and 3.1 s^{-1} is around 80%, whereas for the space velocity of 2.4 s^{-1} is around 90%. Measuring the adiabatic flame temperature while the experiment was performed showed that the maximum observed steady state temperature was 86°C for 2.8 s^{-1} and 3.1 s^{-1} space velocities, whereas the maximum temperature for the 2.4 s^{-1} was around 95°C. Table 4.3 shows the observed maximum temperatures and theoretical reached conversions for 7°C inlet temperature experiments. GC-TCD analysis results are lower than the theoretical conversions. This can be caused because of the carbon dioxide solubility increment at lower temperatures in water. That would be showed the data lower than expected.

Table 4.3. Conditions and calculations for 7°C inlet temperature activity tests.

	2.4 s^{-1}	***2.8 s^{-1}***	***3.1 s^{-1}***
Methanol Mole Amount	3371 ppm	3663 ppm	3880 ppm
Observed Max. Temp.	95 °C	86 °C	86 °C
Theoretical Max. Temp	98 °C	105 °C	111 °C
Theoretical Max. Conversion	~100%	~100%	~100%

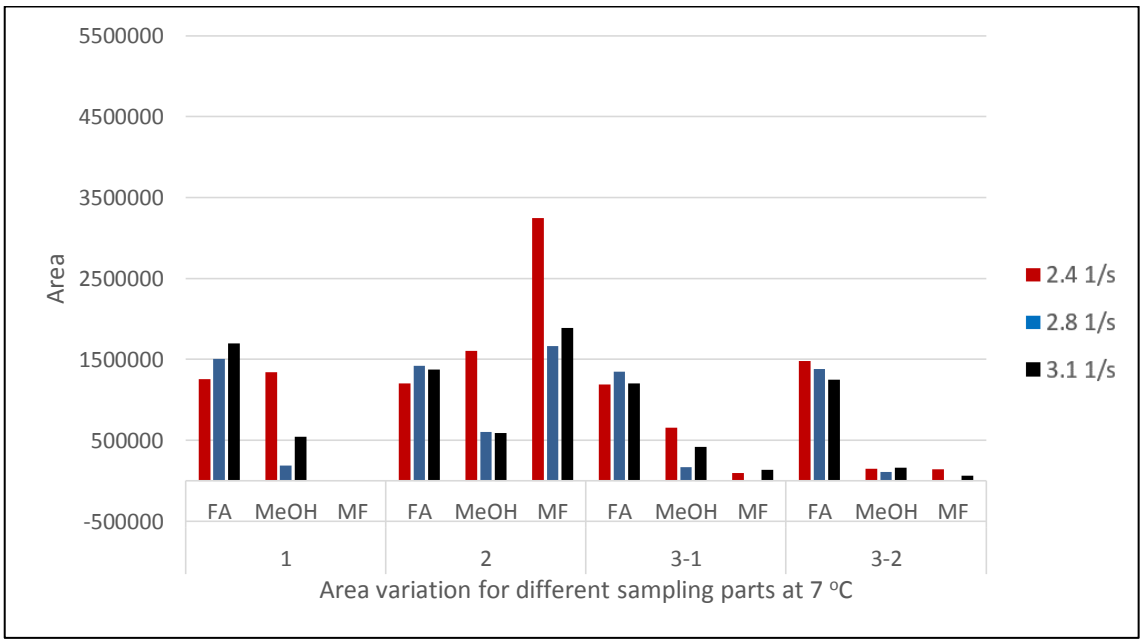

Figure 4.8. GC-MS Reaction behavior at 7°C inlet temperature.

Figure 4.8 shows that unlike room and sub-room inlet temperature results this time at steady parts, the methanol peak is very small. Methanol solubility increases with decreasing temperature as in the case of carbon dioxide. Therefore, methanol could be dissolved in the condensed water droplets at lower temperatures which may led to lower area. On the other hand, methyl formate peak is observed at the end of the reaction, but these peaks are very small like methanol peaks. So that, the same solubility approach can be accepted for methyl formate like methanol. Methyl formate solubility in water increases with decreasing temperature.

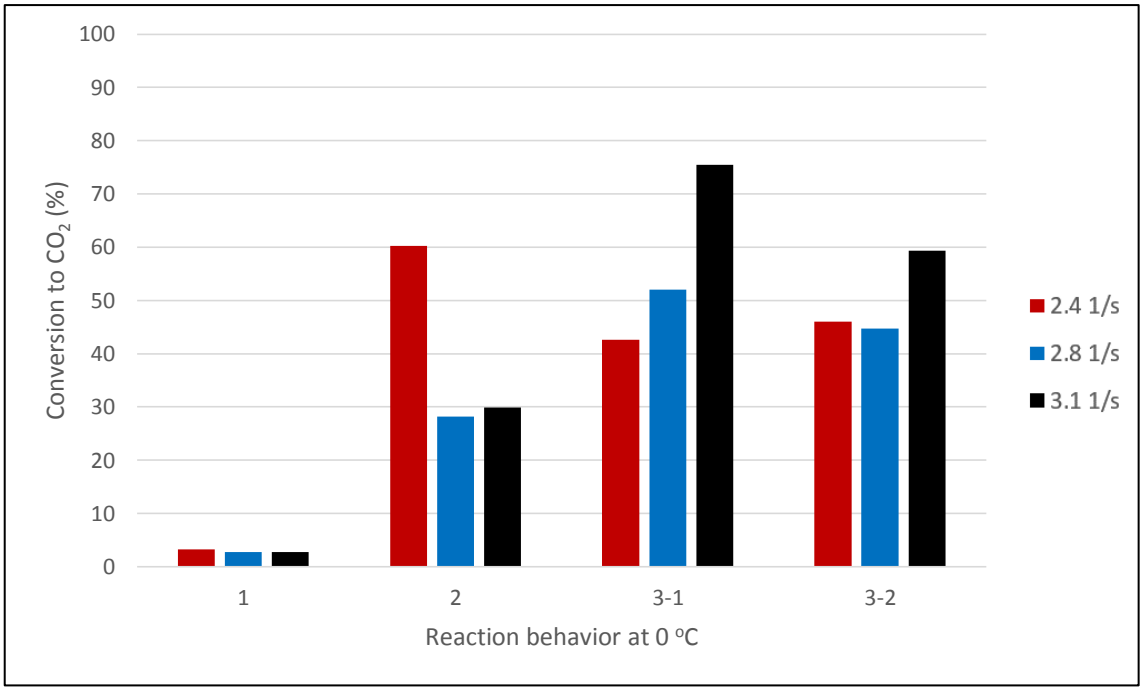

Figure 4.9. Conversion to CO_2 at 0^oC of inlet temperature for all the space velocities.

With the help of the adiabatic flame temperature calculations, theoretical conversions were given in table 4.4. The experiments that were performed at 0^oC inlet temperature, GC-TCD results were given in figure 4.9. Theoretical conversions are around 70%, 70% and 60% for 2.4 s^{-1}, 2.8 s^{-1} and 3.1 s^{-1} space velocities. As in all of the start-up parts of the other experiments, it was showed in figure 4.9, start-up part CO_2 conversion was around 2-3% for all of the space velocities. The steady state CO_2 conversion was around 60% for 3.1 s^{-1} and 45% for 2.4 s^{-1} and 2.8 s^{-1} space velocities. Theoretical calculations and analyzed samples results are not consistent with each other. This inconsistency can be caused because of the little liquid methanol droplets condensation just before the reactor inlet that was resulted with the lowering inlet concentration and led to the lower conversion than expected. Also CO_2 solubility increment in water with decreasing ambient temperature can be caused this too.

Table 4.4. Conditions and calculations for 0°C inlet temperature activity tests.

	2.4 s^{-1}	***2.8 s^{-1}***	***3.1 s^{-1}***
Methanol Mole Amount	3910 ppm	3354 ppm	3373 ppm
Observed Max. Temp.	65 °C	73 °C	65 °C
Theoretical Max. Temp	105 °C	91 °C	91 °C
Theoretical Max Conversion	~100%	~100%	~100%

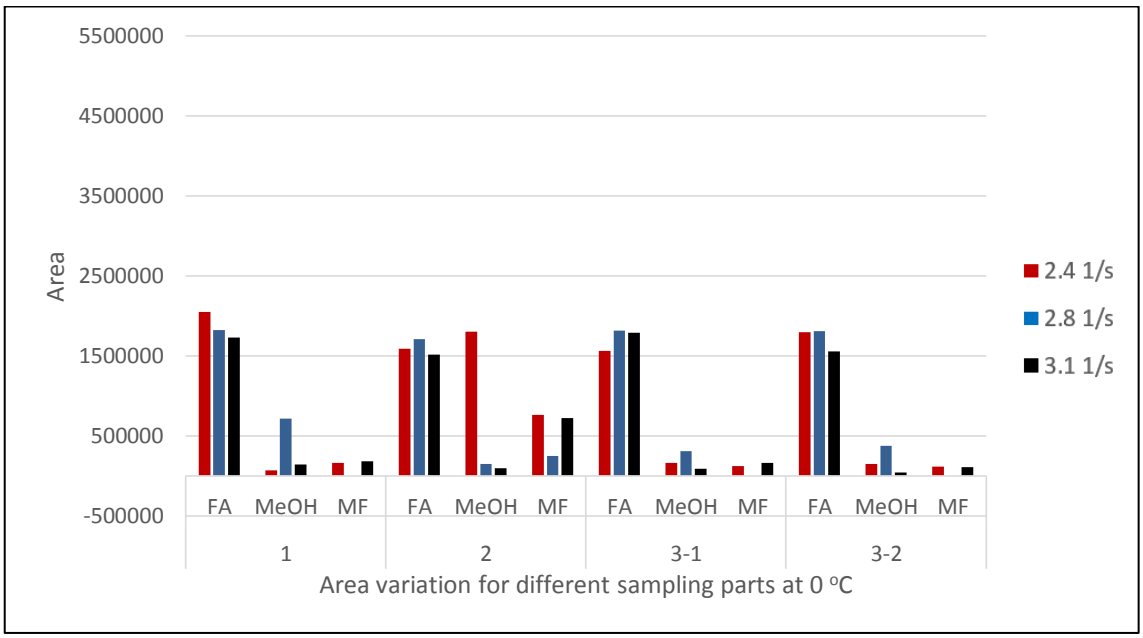

Figure 4.10. GC-MS Reaction behavior at 0°C inlet temperature.

In figure 4.10, it can be seen like as in the case of 7°C GC-MS results, very small methanol peaks were observed at the end of the reaction. This can be caused by the little methanol droplets presence (condensed methanol) throughout the reactor inlet and the increased adsorption of the intermediate species and blocking the active sites of the catalyst surface. In addition to that, increment of the methanol solubility in water with decreasing ambient temperature cannot be estimated. These all can be responsible for the methanol peaks lowering at the end of the reaction. Small peaks of methyl formate were observed at the steady part of the reactions as in the 7°C experiments. And again, methyl formate is produced in the increment part but its amount was lower than the higher temperature experiments.

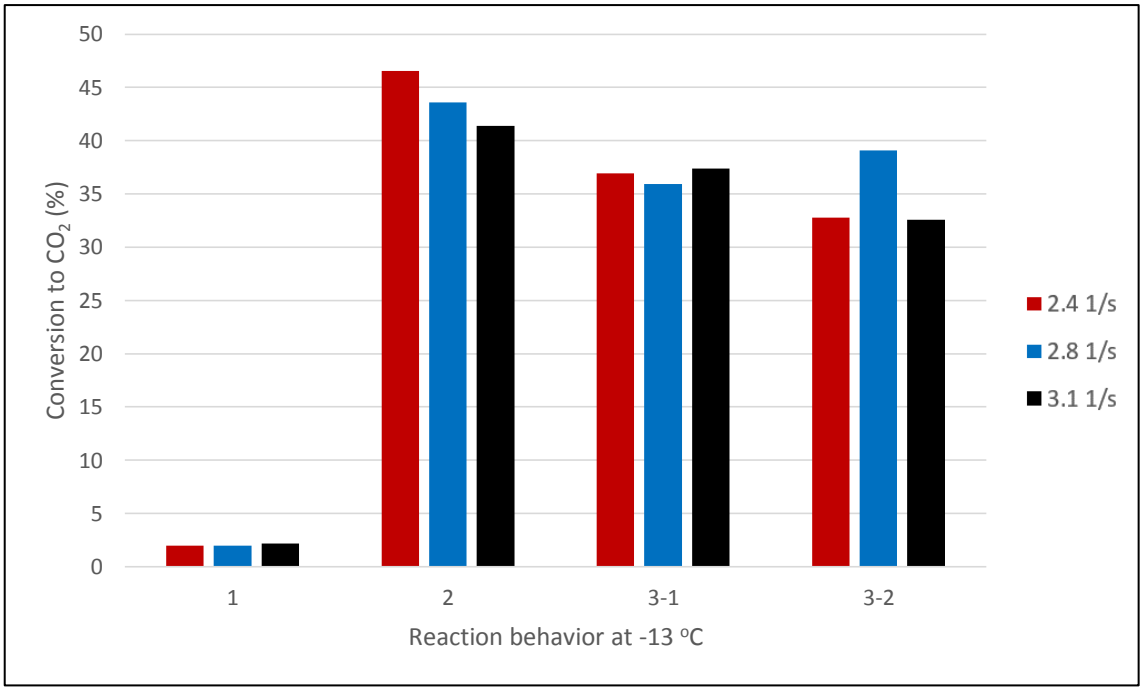

Figure 4.11. Conversion to CO_2 at -13°C of inlet temperature for all the space velocities.

Whether if this catalyst can be used as an external heater for DMFC in special-operations in the military, requiring operating temperature being as low as -20 °C, -13°C inlet temperature experiments were performed. The observed maximum steady state temperatures were 43°C, 49°C and 41°C for 2.4 s^{-1}, 2.8 s^{-1} and 3.1 s^{-1} space velocities, respectively. It was hard to perform this reaction especially in summer months, therefore a different cooler was designed to stay at around this temperature. To simulate the -13°C as in air ambient, the reactor tube was placed about 1 cm higher than the coolers, a little space was left to reflect the air ambient and the system was closed with the glass wool. The temperature was maintained at around -13°C. Analyzed conversions are shown in figure 4.11. At the start-up part the conversions to CO_2 for all three space velocities are around 1-2%. At the increment part the conversions reach between 40-50%. The conversions to CO_2 are found as 35%, 40% and 35% for 2.4 s^{-1}, 2.8 s^{-1} and 3.1 s^{-1} space velocities. On the other hand, theoretical conversions can be seen in table 4.5 and they are higher than the analysis results. Like in 0°C inlet temperature tests, methanol condensation just before the reactor inlet was observed. This can be caused to lowering the inlet methanol concentration, so led to the decrement of the CO_2 analysis results. In addition to that, carbon dioxide solubility increment in water with decreasing

ambient temperature at the exit of the reactor has a responsibility of lowering the analyzed CO_2 results, too.

Table 4.5. Conditions and calculations for -13°C inlet temperature activity tests.

	2.4 s^{-1}	***2.8 s^{-1}***	***3.1 s^{-1}***
Methanol Mole Amount	3380 ppm	3410 ppm	3563 ppm
Observed Max. Temp.	43 °C	49 °C	41 °C
Theoretical Max. Temp	78 °C	79 °C	83 °C
Theoretical Max. Conversion	~100%	~100%	~100%

The long term performance of this catalyst was investigated and it was found that the catalyst reached the same maximum steady state temperature after 19 times usage. In 20th trial the temperature was begun to increase without the methanol flow. That was the indication of the adsorbed species existence on the catalyst surface. Therefore, to remove the adsorbed species, the catalyst was heated in an oven as in the calcination procedure, and reached again the same maximum steady state temperature. That means the deactivation is reversible which is desired.

If we consider all of these behaviors, even at harsh -13°C inlet temperature conditions, utilization of this catalyst in an external heater can help to reach the operation temperature, 50-60°C, of the DMFC. Therefore, we can say that this catalyst is still active below -10°C and feasible to be used as military purposes.

4.3. Catalyst Characterization

X-ray diffraction patterns of the pure alumina, 2% platinum loaded alumina catalyst and activated 2% Pt/Al_2O_3 catalysts are shown in figure 4.12. Both of the inactivated and activated Pt/Al_2O_3 catalysts diffraction pattern is similar to pure alumina. There is not any detected diffraction lines belongs to the platinum crystallites, so that it can be said that crystallite size of the platinum is less than 5nm for both inactivated and activated catalysts. This approach is reasonable since XRD is not sensitive to the crystallite sizes less than 5 nm. In addition to that, in literature there are lots of examples of having small crystallite size leading to the highly dispersed metal

crystallites on the support material surface. Therefore, it can be said that, with respect to the high crystallite sizes, low size of platinum crystallites can be responsible for the better dispersion.

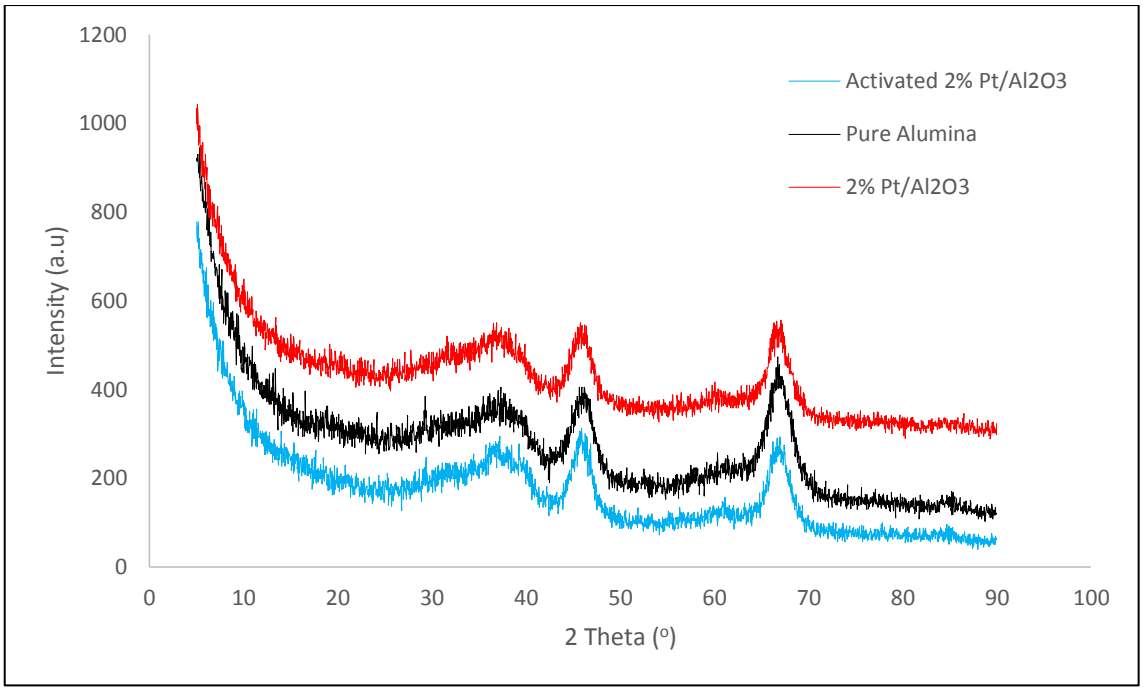

Figure 4.12. XRD pattern of the fresh catalysts

XRD diffraction patterns of the 2% Pt/Al_2O_3 catalyst before the reaction, after the methanol combustion at 28°C for 1 hour and at -13°C for 2 hour are given in Figure 4.13. No change in diffraction patterns of used catalysts were observed as compared to fresh catalyst, which indicates that the crystallite size of Pt stayed constant during the oxidation reactions.

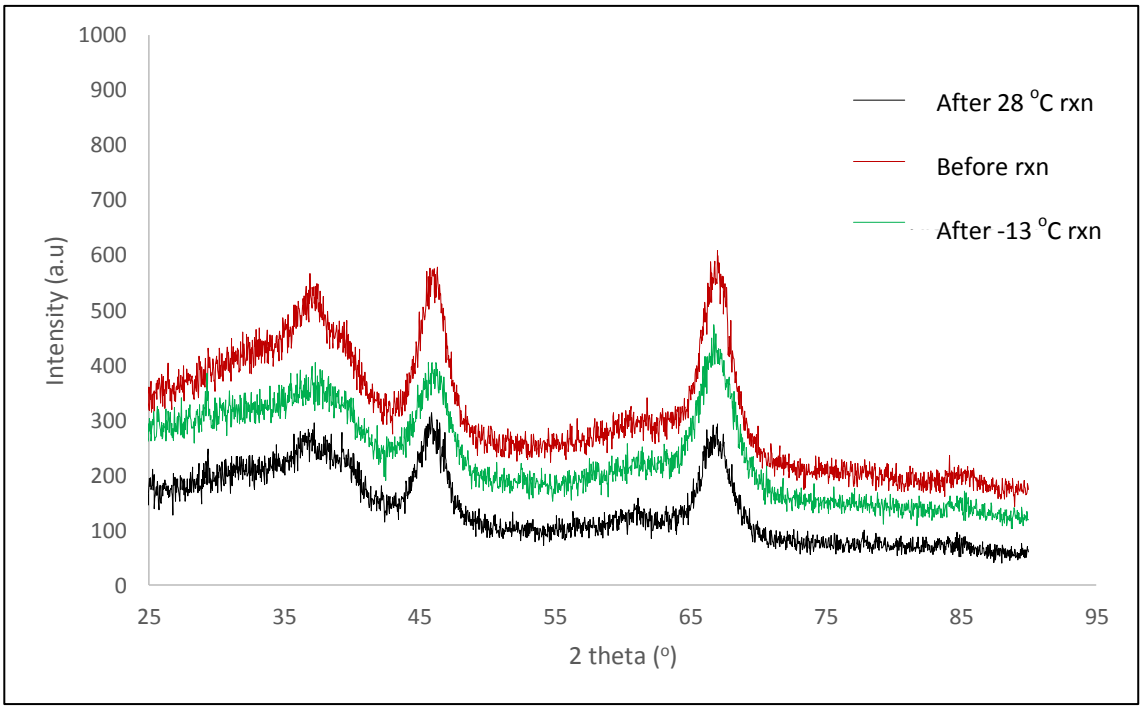

Figure 4.13. XRD pattern of the catalysts (before and after reaction)

On the other hand, BET results showed that the surface area for the fresh catalyst was 246 m^2/g and after the reaction at 28°C, it was 210 m^2/g and after the reaction at -13°C it dropped to 158 m^2/g. Even if the conversion to CO_2 at -13°C inlet temperature experiments are lower than the 28°C inlet temperature experiments, because of the catalyst deactivation by the adsorbed species (e.g. intermediates, methanol) on the catalyst surface and also a possible condensation of the methanol and water over the catalyst surface can caused to the decrement of the surface area at the end of the reactions.

CHAPTER 5

CONCLUSION

In this thesis, the effect of initial temperature and space velocity on the activity and product selectivity of the 2% Pt/Al_2O_3 catalyst was investigated in the combustion of methanol. The product distribution for three different space velocities and five different initial temperatures were studied.

For the room temperature activity tests, 2.4 s^{-1} and 2.8 s^{-1} reflected almost same activity within the error and showed higher activity than 3.1 s^{-1}. This is because of the decreasing conversion/activity with increasing space velocity in packed bed reactor.

The methanol combustion at room temperature (28^oC) and sub-room temperature (15^oC) over the 2% Pt loaded alumina catalyst at all three space velocities resulted in the 100% and 90% conversion to CO_2, respectively. When the combustion of methanol was performed at 7^oC, the conversions decreased to 80% for 2.8 and 3.1 s^{-1} whereas 90% for 2.4 s^{-1}. 0^oC condition conversions were found as around 45% for 2.4 and 2.8 s^{-1} space velocities while the conversion reached 60% at 3.1 s^{-1}. The combustion reaction of methanol was conducted below -10^oC to find out whether if the catalyst is still active at these temperatures. The results showed that the conversion was around 35% for both 2.4 and 3.1 s^{-1} space velocities whereas it was around 40% for 2.8 s^{-1}. At different temperatures, different space velocities conversion was found higher. GC-MS results showed that all of the reactions produced methyl formate intermediate species.

GC-MS results also showed that, for room temperatures and sub-room temperatures, at the end of the methanol combustion reaction, methanol was observed. Even though, its area was much lower than the inlet methanol area, at lower temperatures, that is at 7^oC and 0^oC methanol area was very low. At higher temperatures (28^oC and 15^oC) somehow methanol can be adsorbed somewhere or absorbed by the condensed water droplets, with the continuing flow, then it was most probably desorbed and detected with the GC-MS. At lower temperatures (7^oC and 0^oC), solubility of the methanol in water increases with the decreasing temperature. That seems to be reason for observing lower GC-MS peaks of methanol at 7^oC and 0^oC. In

addition to that, at 0^{o}C and -13^{o}C, methanol condensation just before the reactor inlet was responsible for the inlet methanol concentration which then led the lowering of outlet methanol concentration and CO_2 concentration.

Overall, it can be said that, the catalyst was active even at harsh reaction conditions lower than -10^{o}C. The catalyst is suitable and applicable for low temperature environment heating purposes without using any ignition or external electrical heater but still need improvement in the design of formulation.

REFERENCES

Álvarez-Galván, M.C., Pawelec, B., de la Peña O'Shea, V.A., Fierro, J.L.G., and Arias, P.L. (2004). Formaldehyde/methanol combustion on alumina-supported manganese-palladium oxide catalyst. Applied Catalysis B: Environmental, 51, 83-91.

Aricò, A. S., V. Baglio and V. Antonucci (2009). Direct Methanol Fuel Cells: History, Status and Perspectives. Electrocatalysis of Direct Methanol Fuel Cells, Wiley-VCH Verlag GmbH & Co. KGaA: 1-78.

Arnby, K., Törncrona, A., and Skoglundh, M. (2004). Influence of ammonia on CO and methanol oxidation over Pt/ɣ -Al2O3 catalysts modified by Mg. Applied Catalysis B: Environmental, 49, 51-59.

Badlani, M., Wachs, I. E. (2001). Methanol: A "Smart" Chemical Probe Molecule. Catalysis Letters, 75, 137-149.

Behling, N. H. (2012). Fuel Cells: Current Technology Challenges and Future Research Needs, Elsevier.

Bond, G. C., and Thompson, D. T. (1999). Catalysis by Gold. Catalysis Reviews: Science and Engineering, 41:3-4, 319-388.

Boreskov, G. K., Popovskii, V. V., and Sazanov, V. A. (1971). Proceedings of the Fourth International Congress on Catalysis. Akademia Kiado: Budapest, 1, p. 343.

BP Energy Outlook 2030, january 2013 [cited 2015 February, 17]; Available from: http://www.bp.com/content/dam/bp/pdf/statistical-review/BP_World_Energy_Outlook_booklet_2013.pdf.

Chantaravitoon, P., Chavadej, S., Schwank, J. (2004). Temperature-programmed desorption of methanol and oxidation of methanol on Pt–Sn/Al_2O_3 catalysts. Chemical Engineering Journal, 97, 161-171.

Cordi, E.M. and Falconer, J.L. (1996). Oxidation of Volatile Organic Compounds on Al_2O_3, Pd/Al_2O_3, and PdO/Al_2O_3 Catalysts. Journal of Catalysis, 162, 104-117.

Cordonna, G. W., Kosanovich, M., and Becker, E. R. (1989). Gas Turbine Emission Control, Platinum and Platinum-Palladium Catalysts for Carbon Monoxide and Hydrocarbon Oxidation. Platinum Metals Review, 33, 46-54.

Croy, J. R., Mostafa, S., Liu, J., Sohn, Y., Heinr, H., and Cuenya, B. R. (2007). Support Dependence of MeOH Decomposition over Size-Selected Pt Nanoparticles. Catalysis Letters, 119, 209-216.

Curtin, S., and Gangi, J. (2013). 2013 Fuel Cell Technologies Market Report, Breakthrough Technologies Institute, Inc.

Dönmez, E. (2011). Catalytic Combustion of Methanol on Structured Catalysts for Direct Methanol Fuel Cells, M. Sc. Thesis, Iztech.

Ferrin, P., and Mavrikakis, M. (2009). Structure Sensitivity of Methanol Electrooxidation on Transition Metals. Journal of the American Chemical Society, 131, 14381–14389.

Fuel Cell Market Analysis by Product (PEMFC, DMFC, PAFC, SOFC, MCFC, AFC) and Segment Forecasts To 2020 (2014). Grand View Research, Market Research & Consulting.

Golodets, G. I., Roiter, V. A., and Pyatnitskii, Yu (1971). I. Proceedings of the Fourth International Congress on Catalysis. Akademie Kiado: Budapest, 1, p. 365.

Golodets,G. I. (1983). Heterogeneous Catalytic Reactions Involving Molecular Oxygen. In Studies in Surface Science and Catalysis, Ross, J. R. H. (Ed.), Elsevier: New York, 15, Chapters X and XIV.

Haber, J. Znt. (1975). Chem. Eng., 15, 21.

Hicks, R. F., Lee, R. G., and Han, W. J. (1990). Effect of Catalyst Structure on the Rate of Heptane Oxidation over Platinum and Palladium. Symposium on Structure-Activity Relationships in Heterogeneous Catalysis, Boston, April 22-27.

Hinz, A., Larsson, P.O., Skårman, B. and Andersson, A. (2001). Platinum on alumina, titania, and magnesia supports for the combustion of methanol in a waste gas with trace amount of ammonia. Applied Catalysis B: Environmental, 34 (2), 161-178.

Hinz, A., Larsson, P.O., and Andersson, A. (2002). Influence of Pt loading on Al_2O_3 for the low temperature combustion of methanol with and without a trace amount of ammonia. Catalysis Letter, 78, 177-183.

IEA World Energy Outlook 2012, OECD Publishing. [cited 2015 February, 18]; Available from: https://www.iea.org/publications/freepublications/publication/WEO2012_free.pdf

Imamura, S., Higashihara, T., Saito, Y., Aritani, H., Kanai, H., Matsumura, Y. and Tsuda, N. (1999). Decomposition of Methanol on Pt-loaded Ceria. Catalysis Today, 50 (2), 369-380.

Kizhakevariam, N., and Stuve, E.M. (1993). Promotion and Poisoning of the Reaction of Methanol on Clean and Modified Platinum (100). Surface Science, 286, 246-260.

Lippits, M.J., Boer Iwema, R.R.H., and Nieuwenhuys, B.E. (2009). A comparative study of oxidation of methanol on ɣ -Al2O3 supported group IB metal catalysts. Catalysis Today, 145, 27-33.

Liu, H., Zhang J., (2009). Electrocatalysis of Direct Methanol Fuel Cells, Wiley-VCH Verla –g GmbH & Co.

Luy, J.C., and Parera, J.M., (1984). Selective deactivation of a bifunctional catalyst studied by alcohol decomposition. Applied Catalysis, 13, 39-48.

McCabe, R.W., and Mitchell, P.J., (1986). A Comparative Study of Methanol Oxidation over Alumina-Supported Catalysts Containing Group 9,10, and 11 Metals. Applied Catalysis, 27, 83-98.

Minicò, S., Scirè, S., Crisafulli, C., Maggiore R., and Signorino G. (2000). Catalytic combustion of volatile organic compounds on gold/iron oxide catalysts. Applied Catalysis B: Environmental, 28, 245-251.

Nakagawa, N., and Xiu, Y. (2003). Performance of a direct methanol fuel cell operated at atmospheric pressure. Journal of Power Sources, 118, 248-255.

Ostermaier, J.J., Katzer, J.R. and Manogue, W.H. (1976). Platinum catalyst deactivation in low-temperature ammonia oxidation reactions: I. Oxidation of ammonia by molecular oxygen. Journal of Catalysis, 41, 277-292.

Patterson, A. L. (1939). The Scherrer Formula for X-ray Particle Size Determination. Physical Review, 56, 978 – 982.

Prasad, R., Lawrence, A., Ruckenstein, K. and E. (1984). Catalytic Combustion. Catalysis Reviews: Science and Engineering, 26:1, 1-58.

Sandler, I. S. (2006). Chemical Biochemical and Engineering Thermodynamics, fourth edition, John Wiley & Sons, Inc., 914-931.

Schiffimo R.S., Merrill R.P., 1993, "A Mechanistic Study of the Methanol Dehydration Reaction on Alumina Catalyst", The Journal of Physical Chemistry, Vol. 97, pp. 6425-6435

Sexton, B.A. (1981). Methanol Decomposition on Platinum (111). Surface Science, 102, 271-281.

Shah, R. K. (2007). Recent Trends in Fuel Cell Science and Technology, Suddhasatwa Basu (Ed.). Springer New York.

Sharma, R. K., Zhou, B., Tong, S., and Chuang, K.T. (1995). Catalytic Destruction of Volatile Organic Compounds Using Supported Platinum and Palladium Hydrophobic Catalysts. Industrial & Engineering Chemistry Research, 34, 4310-4317.

Silva F.A., Martinez D.S., Ruiz J.A.C, Mattos L.V, Noronha F.B., Horia C.E., 2007, "The Effect of Pt Loading and Space Velocity on the Performance of Pt/CeZrO2/Al2O3 Catalysts for the Partial Oxidation of Methane", Natural Gas Conversion VIII, Vol. 167, pp. 427-432

Simons. T. G. J., Verhiien, E. J. M., Batist, P. A., and Schuit, G. C. A. (1968). Adu.'Chem. Ser., 76, 261.

Spearrin, M., 2012, Methanol: An Alternative Transportation Fuel [cited 2015 February, 20]; Available from: http://large.stanford.edu/courses/2012/ph240/spearrin2/

Spivey, J. J. (1987). Complete catalytic oxidation of volatile organics. Industrial & Engineering Chemistry Research, 26, 2165-2180.

Spivey, J. J., and Roberts, G. W. (2004). "Catalysis", The Royal Society of Chemistry, 17, 1-115.

Srinivasan, S. (2006). Fuel Cells: From Fundamentals to Applications, Springer.

The Fuel Cell Industry Review 2012. [cited 2015 February, 20]; Available from: http://www.fuelcelltoday.com/media/1713685/fct_review_2012.pdf.

The Fuel Cell Industry Review 2013. [cited 2015 February, 20]; Available from: http://www.fuelcelltoday.com/media/1889744/fct_review_2013.pdf

Web-1. World Fuel Cells, 2015 [cited 2015 March, 4]; Available from: http://www.freedoniagroup.com/industry-study/2502/world-fuel-cells.htm.

Wang, J., DeAngelis, M.A., Zaikos, D., Setiadi, M., and Masel, R.I. (1994). Methanol Oxidation on (2×1) Pt (110): Formaldehyde on a Stepped Surface. Surface Science, 318, 307-320.

World Fuel Cells, May 2009, Industry Study with Forecasts for 2013 & 2018. [cited 2015 March, 6]; Available from: http://www.freedoniagroup.com/brochure/25xx/2502smwe.pdf

Xu, K., Pierce, D.T., Li, A., and Zhao, J. X. (2008). Nanocatalysts in Direct Methanol Fuel Cell Applications. Synthesis and Reactivity in Inorganic, Metal-Organic, and Nano-Metal Chemistry, 38, 394–399.

APPENDIX A

ADIABATIC FLAME TEMPERATURE CALCULATION

Methanol combustion reaction;

The dry air can be approximated as 21 percent oxygen and 79 percent nitrogen by mole numbers. Therefore, each mole of oxygen entering a combustion chamber is accompanied by 0.79/0.21= 3.762 mol of nitrogen. That is,

1 mol O_2 + 3.762 mol N_2= 4.762 mol air

Assumptions:

- The system is at steady state
- There is no heat loss, Q=0, because reactor was insulated.
- No work is produced W=0
- The combustion products contain CO_2, H_2O, O_2, and N_2 only
- Combustion is complete

In order to find the adiabatic flame temperature, initially the energy balance is written as;

$$Q + W = \sum_{i=1}^{c} N_i \; in \int_{T_{in}}^{T_{ad}} C_{P,i}\, dT + \sum_{j=1}^{M} \Delta_{rxn,j} H(T_{ad}) \; X_j \qquad (1)$$

In the equation 1, Q=0 and W=0 therefore the left side of the equation equals to zero;

$$\underset{0}{\cancel{Q}} + \underset{0}{\cancel{W}} = \sum_{i=1}^{c} N_i \; in \int_{T_{in}}^{T_{ad}} C_{P,i}\, dT + \sum_{j=1}^{M} \Delta_{rxn,j} H(T_{ad}) \; X_j$$

$$0 = \sum_{i=1}^{c} N_i \; in \int_{T_{in}}^{T_{ad}} C_{P,i}\, dT + \sum_{j=1}^{M} \Delta_{rxn,j} H(T_{ad}) \; X_j \qquad (2)$$

To find the $\Delta_{rxn,j}H$ the following equation was used;

$$\Delta_{rxn} H^o \; T, 1bar \; = \Delta_{rxn} H^o \; 25^o C, 1\; bar \; + \; {}_i v_i \int_{T=25^o C}^{T_{ad}} C^o{}_{P,i}\, dT \qquad (3)$$

$\Delta_{rxn}H\ 25^oC\ = h_c$, thus the heat of combustion $h_c = H_{product} - H_{reactant}$ was calculated by using the values of heat of formation of substances.

$$h_c = H_{product} - H_{reactant} \longrightarrow h_c = N_p h^o{}_{f,p} - N_r h^o{}_{f,r} \quad (4)$$

The heat of formation of substances (at 25°C and 1 atm) was given in Table A.1.

Table A.1. Heat of formation of substances
(Source: Sandler, 2006)

Substances	$\Delta_f \underline{H}^o$ of the substance (j/mol)
CO_2	-393500
H_2O	-241800
CH_3OH	-200700
O_2	0
N_2	0

The heat of formation of the elements is zero, thus $\Delta_f \underline{H}^o$ of O_2 and N_2 is zero in the table A.1.

Besides, the heat capacities were calculated by using the equation 5 and the heat capacity constants were given in Table A.2.

$$C_p = a + bT + cT^2 + dT^3 \quad (5)$$

Table A.2. The heat capacity constants
(Source: Sandler, 2006)

	Cp values (J/mol K)				
	CO_2	H_2O	CH_3OH	O_2	N_2
a	2.22E+01	32.218	19.038	25.46	28.883
b	5.98E-02	1.92E-03	9.15E-02	1.52E-02	-1.57E-03
c	-3.50E-05	1.06E-05	-1.22E-05	-7.15E-06	8.08E-06
d	7.46E-09	-3.59E-09	-8.03E-09	1.31E-09	-2.87E-09

After the heat of reaction and heat capacity calculations, equation 2 was used and the adiabatic flame temperature was calculated for a given methanol conversion.

Table A.3. Adiabatic flame temperature vs. conversion for 28°C inlet temperature

For 28 °C Inlet Temperature										
	3100 ppm									
%	100	90	80	70	60	50	40	30	20	10
°C	110	102	93	85	77	69	61	53	44	36
	3300 ppm									
%	100	90	80	70	60	50	40	30	20	10
°C	118	109	100	91	82	73	64	55	46	37

Table A.4. Adiabatic flame temperature vs. conversion for 15°C inlet temperature

For 15 °C Inlet Temperature										
	3396 ppm									
%	100	90	80	70	60	50	40	30	20	10
°C	106	97	88	79	70	61	52	42	33	24
	3905 ppm									
%	100	90	80	70	60	50	40	30	20	10
°C	120	109	99	88	78	68	57	47	36	26

Table A.5. Adiabatic flame temperature vs. conversion for 7°C inlet temperature

For 7 °C Inlet Temperature										
	3371 ppm									
%	100	90	80	70	60	50	40	30	20	10
°C	98	88	79	70	61	52	43	34	25	16
	3663 ppm									
%	100	90	80	70	60	50	40	30	20	10
°C	105	95	85	75	66	56	46	37	27	16
	3880 ppm									
%	100	90	80	70	60	50	40	30	20	10
°C	110	100	90	79	69	59	48	38	28	17

Table A.6. Adiabatic flame temperature vs. conversion for 0°C inlet temperature

For 0 °C Inlet Temperature										
	3354 ppm									
%	100	90	80	70	60	50	40	30	20	10
°C	90	81	72	63	54	45	63	27	18	9
	3910 ppm									
%	100	90	80	70	60	50	40	30	20	10
°C	105	94	83	73	63	52	42	31	21	10

Table A.7. Adiabatic flame temperature vs. conversion for -13^{o}C inlet temperature

For -13 ^{o}C Inlet Temperature										
	3380 ppm									
%	100	90	80	70	60	50	40	30	20	10
^{o}C	77	68	59	50	41	32	23	14	5	-4
	3560 ppm									
%	100	90	80	70	60	50	40	30	20	10
^{o}C	83	73	63	54	44	35	25	16	6	-3

APPENDIX B

AVERAGE FLOW RATE & METHANOL MOLE AMOUNT

Table B.1. 28°C inlet temperature & 2.4 s^{-1} space velocity

28°C			
2.4 s^{-1}			
DA (ml/min)	HE (ml/min)	HE+MEOH (ml/min)	
26.3	24.6	24.8	
26.5	24.7	24.9	
26.4	24.7	24.8	
26.4	24.7	25	
26.5	24.7	24.8	
26.6	24.7	24.9	
26.4	24.7	24.8	
26.44	**24.69**	**24.86**	mole %
		0.17	**0.33**

Table B.2. 28°C inlet temperature & 2.8 s^{-1} space velocity

28°C			
2.8 s^{-1}			
DA (ml/min)	HE (ml/min)	HE+MEOH (ml/min)	
26.3	24.7	24.8	
26.2	24.6	24.9	
26.3	24.6	24.8	
26.4	24.6	24.8	
26.3	24.6	24.8	
26.4	24.7	24.8	
26.3	24.7	24.7	
26.31	**24.64**	**24.8**	mole %
		0.16	**0.31**

Table B.3. 28°C inlet temperature & 3.1 s^{-1} space velocity

28°C			
3.1 s^{-1}			
DA (ml/min)	**HE (ml/min)**	**HE+MEOH (ml/min)**	
26.6	24.8	24.9	
26.8	24.8	24.8	
26.8	24.7	24.9	
26.7	24.7	25	
26.8	24.8	24.8	
26.8	24.8	25.1	
26.6	24.8	25.1	
26.73	**24.77**	**24.94**	mole %
		0.17	**0.33**

Table B.4. 15°C inlet temperature & 2.4 s^{-1} space velocity

15°C	AF 10 °C	
2.4 s^{-1}	Air 15 °C	
DA (ml/min)	**HE (ml/min)**	**HE+MEOH (ml/min)**
25.6	24.7	24.9
25.7	24.8	25
25.5	24.7	25
25.4	24.7	24.8
25.4	24.8	24.8
25.7	24.8	25.1
25.6	24.7	24.8
25.56	**24.74**	**24.91** mole %
		0.17 **0.34**

Table B.5. 15°C inlet temperature & 2.8 s^{-1} space velocity

15°C	AF 9 °C		
2.8 s^{-1}	Air 14 °C		
DA (ml/min)	**HE (ml/min)**	**HE+MEOH (ml/min)**	
26	24.9	25.2	
25.7	25	25.2	
25.6	25	25.2	
25.7	25	25.1	
25.8	24.9	25.2	
25.7	24.9	25.1	
25.8	25	25.1	
25.76	**24.96**	**25.18**	mole %
		0.2	0.39

Table B.6. 15°C inlet temperature & 3.1 s^{-1} space velocity

15°C	AF 9 °C		
3.1 s^{-1}	Air 14 °C		
DA (ml/min)	**HE (ml/min)**	**HE+MEOH (ml/min)**	
25.8	25.2	25.4	
25.8	25.2	25.5	
25.8	25.2	25.5	
25.9	25.3	25.4	
25.7	25.2	25.4	
25.8	25.2	25.4	
25.8	25.2	25.3	
25.8	**25.21**	**25.41**	mole %
		0.2	0.39

Table B.7. 7°C inlet temperature & 2.4 s^{-1} space velocity

7°C	AF 2 °C	
2.4 s^{-1}	Air 3 °C	
DA (ml/min)	**HE (ml/min)**	**HE+MEOH (ml/min)**
26.1	24.6	24.9
25.9	24.6	24.8
26.2	24.7	24.7
26.2	24.6	24.8
25.9	24.6	24.9
26.1	24.6	24.8
25.9	24.7	24.7
26.04	**24.63**	**24.8** mole %
		0.17 **0.34**

Table B.8. 7°C inlet temperature & 2.8 s^{-1} space velocity

7°C	AF 2 °C	
2.8 s^{-1}	Air 4 °C	
DA (ml/min)	**HE (ml/min)**	**HE+MEOH (ml/min)**
26.1	24.2	24.4
26.3	24.2	24.5
26.3	24.3	24.6
26.2	24.4	24.5
26.3	24.4	24.5
26.2	24.3	24.4
26.2	24.2	24.4
26.23	**24.29**	**24.47** mole %
		0.18 **0.37**

Table B.9. 7°C inlet temperature & 3.1 s^{-1} space velocity

7°C	AF 2 °C	
3.1 s^{-1}	Air 3 °C	
DA (ml/min)	**HE (ml/min)**	**HE+MEOH (ml/min)**
26.4	25	25.1
26.3	24.9	25.1
26.4	25.1	25.3
26.4	24.9	25.1
26.5	24.9	25.3
26.3	25	25.1
26.4	24.9	25.1
26.39	**24.96**	**25.16**	mole %
		0.2	**0.39**

Table B.10. 0°C inlet temperature & 2.4 s^{-1} space velocity

0°C	AF -13 °C	
2.4 s^{-1}	Air -3 °C	
DA (ml/min)	**HE (ml/min)**	**HE+MEOH (ml/min)**
26.3	24.6	24.7
26.3	24.6	24.8
26.4	24.5	24.8
26.4	24.6	24.9
26.4	24.5	24.8
26.5	24.6	24.7
26.4	24.6	24.7
26.39	**24.57**	**24.77**	mole %
		0.2	**0.39**

Table B.11. 0°C inlet temperature & 2.8 s^{-1} space velocity

0 °C	AF -13 °C		
2.8 s^{-1}	Air -3 °C		
DA (ml/min)	**HE (ml/min)**	**HE+MEOH (ml/min)**	
26.3	24.8	25	
26.3	24.8	24.9	
26.1	24.8	25.1	
26.3	24.7	25	
26.1	24.7	24.8	
26.2	24.7	24.9	
26	24.8	24.8	
26.19	**24.75**	**24.93**	mole %
		0.17	**0.34**

Table B.12. 0 °C inlet temperature & 3.1 s^{-1} space velocity

0 °C	AF -13 °C		
3.1 s^{-1}	Air -3 °C		
DA (ml/min)	**HE (ml/min)**	**HE+MEOH (ml/min)**	
26.1	24.6	24.7	
26	24.7	24.8	
26	24.6	24.8	
26	24.7	24.8	
26.1	24.7	24.9	
26	24.6	24.9	
25.9	24.6	24.8	
26.01	**24.64**	**24.81**	mole %
		0.17	**0.34**

REFERS TO:

DA: DRY AIR FLOW RATE

HE: HELIUM FLOW RATE

HE+MEOH: HELIUM + METHANOL FLOW RATE

AF: ANTI-FREEZE TEMPERATURE

AIR: SIMULATED AIR TEMPERATURE

YELLOW BACKGROUND: INLET TEMPERATURE

RED BACKGROUND: AVERAGE METHANOL FLOW RATE

BLACK BACKGROUND & RED FONT COLOR: SPACE VELOCITY

PURPLE BACKGROUND: METHANOL MOLE AMOUNT